Effects of Fuel Split Ratio on NO_x Emissions of a Lean-burn Staged Combustor

by

Yang Chen

Submitted to the Department of Aeronautics and Astronautics
in partial fulfillment of the requirements for the degree of

Master of Science in Aeronautics and Astronautics

at the

MASSACHUSETTS INSTITUTE OF TECHNOLOGY

May 2022

© Massachusetts Institute of Technology 2022. All rights reserved.

Author .....
Department of Aeronautics and Astronautics
May 17, 2022

Certified by .....
Raymond Speth
Principal Research Scientist
Thesis Supervisor

Accepted by .....
Jonathan P. How
R. C. Maclaurin Professor of Aeronautics and Astronautics
Chair, Graduate Program Committee

Effects of Fuel Split Ratio on NO_x Emissions of a Lean-burn Staged Combustor

by

Yang Chen

Submitted to the Department of Aeronautics and Astronautics
on May 17, 2022, in partial fulfillment of the
requirements for the degree of
Master of Science in Aeronautics and Astronautics

Abstract

Aviation NO_x emissions are a significant factor in causing air quality deterioration, leading to potentially 16,000 annual premature deaths globally. To cope with the expected increase in air traffic demand in the near future, aircraft-based lean-burn staged combustion becomes a promising solution in reducing NO_x emissions. This thesis investigates the effects of a lean-burn staged combustor's fuel split ratio and staging threshold on the NO_x emissions for both a sea-level static scenario and a representative flight mission. NO_x reduction benefits from optimizing the fuel split ratio are studied, and the EI_{NO_x} performance between an RQL and a lean-burn staged combustor are compared. Chemical reactor networks, NPSS engine cycle models, and a TASOPT flight mission model are utilized. In comparison to previous studies, a wider range of pilot fuel fraction, from 16% to 100%, are tested over more refined thrust cases, from 0% to 100% rated thrust. A wider range of phases, including the cruise conditions in addition to the LTO cycle, is employed in this thesis. This thesis illustrates how a pilot fuel fraction below 30% is infeasible through the calibration of the combustor model. It is found that staging should occur as early as allowed by combustion stability to minimize NO_x emissions, and the optimal fuel split ratio is roughly constant across different throttle conditions. Moreover, reducing the air distributed to the pilot zone decreases the overall EI_{NO_x} level, and the lean-burn staged combustor is observed to outperform an RQL combustor in terms of NO_x emissions.

Thesis Supervisor: Raymond Speth
Title: Principal Research Scientist

Acknowledgments

I would like to thank my advisor, Ray, for his guidance and support over the past two years and also my colleagues from Laboratory for Aviation and the Environment. Thank you all very much for making our lab a better place. In addition, I would like to thank FAA's ASCENT Center of Excellence for funding support.

Contents

List of Figures

List of Tables

Chapter 1

Introduction

The primary pollutants out of aircraft engine include unburnt HC, NO_x, CO, Particulate Matter (PM), and CO_2 [3]. Among those, NO_x emissions have been a significant factor in causing air quality deterioration through the creation of ozone and $PM_{2.5}$. It has been shown that most of the aviation-induced $PM_{2.5}$ emissions at the sea level are formed through the reaction of background ammonia with NO_x or SO_x emitted by aircraft [4, 5]. In addition, NO_x contributes significantly to the creation of troposphere's ozone due to its high residence time at altitude and its reactions with background unburnt HC [6]. On the sea level, the created $PM_{2.5}$ and ozone increase the rates of cardiovascular and respiratory diseases, and it has been estimated that around 16,000 annual premature deaths can be attributed to aviation, with 9,200 of them from $PM_{2.5}$ and the rest from ozone [4, 7]. After the COVID-19 pandemic, air traffic demand is expected to grow back to its pre-crisis level in the near future with an estimated annual growth rate of 3.6% to 4% for the following 20 years [8, 9, 10]. Hence, aviation NO_x emissions shall continue to be an important topic of consideration for the aviation industry.

To alleviate the problem with aviation NO_x emissions, the International Civil Aeronautics Organization (ICAO) since 1986 has been continuously imposing more stringent requirements on the NO_x emissions of aircraft engines [11]. Different low emission propulsion technologies have been developed since then. As for combustion technologies, designs can be grouped into two categories, a rich-burn and a lean-burn

process. Examples of the rich-burn technology include the Low-Emission Combustor (LEC) from 1970s and the Rich-burn Quick-quench Lean-burn Combustor (RQL) from 1980s [11]. They both follow the main principle of burning initially in rich conditions such that only limited air can contribute to the formation of NO_x. The main difference between them is the rate of mixing of the cooling air with the rich-burn products. On the other hand, examples of the lean-burn technology include the Double Annular Combustor (DAC) from 1970s and the Twin Annular Premixing Swirler Combustor (TAPS) from 1995 [11]. They rely on the lean-burn low combustion temperature to reduce NO_x emissions, while the level of uniformity of the internal temperature and species concentration fields are different between them.

Among these combustors, the TAPS combustor has been of great research interest potentially due to its staged combustion process and its more recent adoption onto aircraft engines. The TAPS combustor consists of a radially inward fuel injector creating a pilot diffusion flame and a radially outward fuel injector creating a main partially-premixed flame [11]. During high power operation, both flames are operating in lean conditions to avoid the high NO_x emissions from a high-temperature stoichiometric combustion. However, during low power operation, fuel is only supplied to the pilot fuel injector to sustain a more stable diffusion flame [12]. RQL combustors have been incorporated into the CFM56-5B and -7B engines certificated in 2005 and 2006 among other applications. In comparison, the TAPS combustor on the GEnx engine was certificated in 2012, and the further developed smaller version TAPS II combustor was adopted by the LEAP-1A and -1B engines certificated in 2016 and used on Airbus A320neo and Boeing 737Max airplanes [1].

As a diffusion flame tends to create a high temperature stoichiometric region accompanied by a high NO_x production rate [3], the fuel distribution between the main and the pilot flame is an important parameter for the low emission design of a staged combustor. The percentage of fuel flowing through the pilot fuel injector over the total fuel delivered to the combustor is the pilot fuel fraction. Previous studies have been done on understanding the effects of the pilot fuel fraction on NO_x emissions, stability, and combustion efficiency. Yamamoto et al. [13, 14, 15] have utilized

the stability-required minimum pilot fuel fraction for each of their combustor power levels, though the detailed effects of this fraction on emissions were not discussed extensively. Through CFD and experimental studies, NO_x emissions were observed to monotonically decrease with the reduction of pilot fuel fraction by Fu et al. [16] and Zhichao et al. [17], so the optimal fraction is determined mainly by combustion stability instead. However, a non-zero optimal pilot fuel fraction for minimum NO_x emissions was discovered by Cheng et al. [18] and Liu et al. [19] through CFD, experiment, and chemical reactor network analysis. This phenomenon was explained as an overly-suppressed pilot fuel fraction resulting in a near-stoichiometric main flame with a high NO_x production rate [19]. Li et al. found that the optimal pilot fuel fraction for minimum NO_x emissions actually varied for different engine power levels, and the minimum NO_x production was achieved by keeping a constant maximum main flame equivalence ratio of around 0.69 [20]. Besides these studies performed on aircraft engine combustors, the optimal pilot fuel fraction for low NO_x operation has also been studied for ground-level industrial gas turbine combustors, where the optimal fractions discovered were relatively low ($< 5\%$) in comparison to aircraft engines [21, 22], while the same principle of low and uniform temperature field resulting in low NO_x emissions was demonstrated.

Given the previous studies, multiple areas of improvement are proposed for this thesis. First, most of the previous studies utilized only a few combustor inlet conditions and engine thrust levels for testing. Even from the study with the most comprehensive range of test conditions, only six cases were used to simulate the effects of the pilot fuel fraction across four distinct T_{t3} levels and four different fuel air ratios. Testing with more combustor inlet conditions provides a more robust argument on the effects of the pilot fuel fraction. Second, previous studies focused primarily on only pilot fuel fractions ranging from 0% to 30% [18, 19, 20], while testing with fractions from 30% to 50% may provide additional useful insights. Third, previous research evaluated the combustor performance during the pilot-only and the main-also modes individually, while when the combustor should switch from the pilot-only mode to the main-also mode (staging threshold) is also worth studying. In this work,

the pilot-only mode refers to the low power operation when the fuel is supplied only to the pilot fuel injector, and the main-also mode refers to the high power operation when the fuel is supplied to both the pilot and the main fuel injectors. The term "staging" refers to the process of switching from the pilot-only mode to the main-also mode. This staging threshold has been loosely defined previously [12] as somewhere between the approach and the climb-out thrust levels.

Hence, this thesis aims at understanding the effects of the pilot fuel fraction ranging from 0% to 50% on the NO_x emissions for a lean-burn staged combustor across different throttle conditions ranging from 0% to 100% rated thrust. An optimal pilot fuel fraction with minimum NO_x emissions is determined for each throttle condition. Although the air distribution between the pilot and the main zones is mostly predetermined by the combustor geometry and can hardly be changed in flight, the effects of the air distribution on the optimal pilot fuel fraction are still studied in terms of how the geometry of the combustor can affect NO_x emissions. Analyses are performed for both the in-flight and the sea-level static operations of the combustor, when the staging threshold is also studied. In addition, the EI_{NO_x} performance between an RQL and the lean-burn staged combustor are compared. Because previous studies have successfully applied chemical reactor networks with detailed reaction mechanisms to simulate the NO_x, CO, and soot emissions from an RQL combustor [23, 24, 25, 26, 27] and a lean-burn staged combustor [19], this technique is also selected for this thesis.

Chapter 2

Methodology

This section first discusses the construction of a combustor model (chemical reactor network) for a lean-burn staged combustor. The flame structure is introduced, based on which the general reactor network layout is arranged. Then, the detailed equations for each reactor are explained, followed by a higher level overview of how the combustor model is operated and calibrated to represent a realistic combustor. The combustor inlet conditions are explained at the end of this section, followed by a discussion on a TASOPT flight mission model and an NPSS engine cycle model that are used. The combination of these two models provides combustor inlet conditions.

2.1 Flame Structure

To create a chemical reactor network for a lean-burn staged combustor, it is critical to first understand the general flame structure within. A schematic of a lean-burn staged combustor is shown in Figure 2-1. At the front end of the combustor, there exist three air passages and two fuel injectors, radially distributed. Two of the air passages and one of the fuel injectors near the center-line produce a non-premixed pilot flame, while the other two produce a partially-premixed main flame [28]. On the side of the combustor, a liner cooling flow exists, carrying roughly 30% of the total combustor air flow [12]. A step circulation zone is observed between the roots of the two flames which is important for combustion stability. Near the center-line,

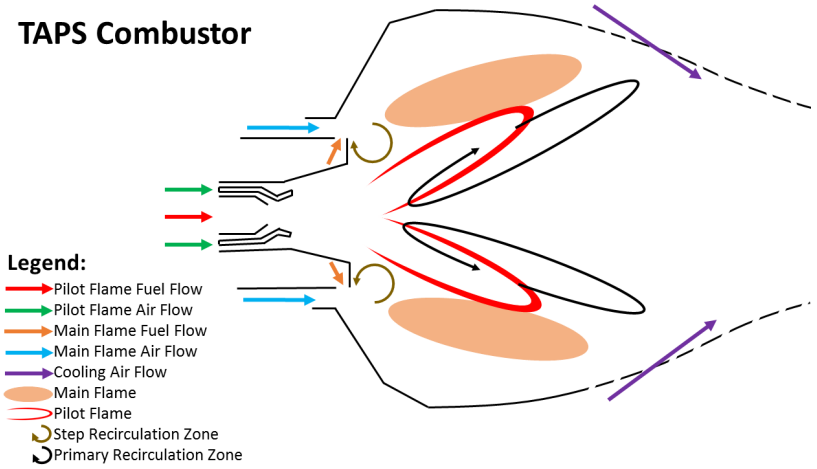

Figure 2-1: Schematic of a lean-burn staged combustor

a primary recirculation zone overlaps with the inner part of the pilot flame [29], indicating the level of mixing within the pilot flame.

Unlike an RQL combustor that utilizes the rich-burn process to achieve high combustion stability and low NO_x emissions, a lean-burn staged combustor relies on a uniform lean flame to achieve the same goal. At high power conditions, both the pilot and the main flames have overall equivalence ratios lower than one [12]. Due to the relatively low and uniform temperature field [30] and the lack of need to quench the flow through the stoichiometric fuel air ratio [12], the partially premixed lean-burn main flame incurs low NO_x emissions. However, because lean-burn is susceptible to instability [31], the non-premixed pilot flame is needed during high power operation to stabilize the main flame and enhance the combustion efficiency [19]. During low throttle operation, the main fuel injector is turned off, and only a rich-burn non-premixed pilot flame exists to maintain combustion stability [16]. This process of turning on the main fuel injector when switching from low power to high power operation is termed "staging" in this study.

Although the pilot diffusion flame containing a high temperature flame sheet tends to have a high NO_x production rate, the total pilot NO_x emissions can be controlled by instead passing most of the combustor air and fuel flows to the main flame [30]. In addition, the overall lean-burn process enables low nvPM emissions [30]. As a result, a highly stable and efficient combustion process with low emissions can be realized

by a lean-burn staged combustor.

2.2 Chemical Reactor Network

Based on the flame structure from Figure 2-1, a chemical reactor network is proposed as shown in Figure 2-2. For the pilot flame root, due to the primary recirculation zone that enhances the mixing of the fresh pilot fuel and air with the hot burnt products, well stirred reactors (WSR) are employed to model this region [29]. However, representing the whole region with one single WSR is unrealistic, because the separate non-premixed injections of the pilot fuel and air result in multiple small pockets of combustible mixture, each with a distinct equivalence ratio that cannot all be represented by a homogeneous mixture [32, 33]. Thus, as successfully utilized by previous studies [26, 23], a non-uniform well stirred reactor is employed to represent the pilot flame root in this work. The non-uniform well stirred reactor contains multiple smaller well stirred reactors, each with a unique equivalence ratio, whose details are explained in the next section.

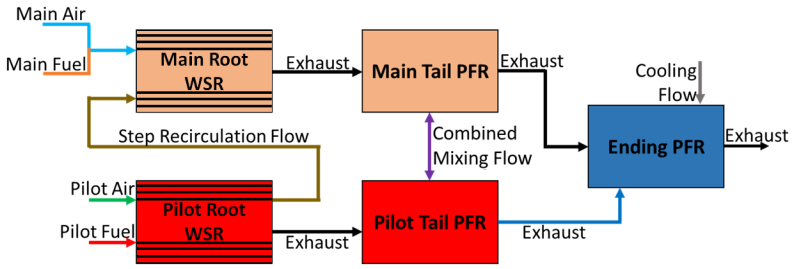

Figure 2-2: Chemical reactor network of a lean-burn staged combustor

The exhaust of the pilot root WSR splits into two branches. One branch is the trailing part of the pilot flame which is represented by the pilot tail plug flow reactor (PFR). The other branch called the step recirculation flow (SRF) goes to the main flame root. As indicated by the name, the step recirculation flow represents the hot products carried by the step recirculation zone from the pilot flame root to the main flame root. As the main stream is observed to be ignited beyond the region where it overlaps the pilot flame, it is believed that the step recirculation zone is important to

the stabilization of the main flame [29].

As the main flame is partially premixed [29], it is assumed that the fuel and the air flows are mixed into a semi-homogeneous mixture before entering the main zone. However, it is uncertain whether the step recirculation flow can be ideally mixed into the main zone fuel air mixture, because the mixing is caused by shear between the pilot and the main streams and is susceptible to oscillation. Thus, similar to the pilot zone, a non-uniform well stirred reactor is adopted to model the main flame root, while each well stirred reactor component carries a unique combination of the fresh main flame fuel air mixture and the step recirculation flow.

The exhaust from the main root WSR becomes the trailing part of the main flame, represented by the main tail PFR. The trailing parts of both flames can be located in Figure 2-1 as the sections where the pilot flame touches the main flame. Based on PIV, formaldehyde PLIF, and CFD data from previous studies, downstream of the step recirculation zone, the pilot flame merges with the main flame, and the flow is also observed to be more uniform in this overlapping region than the regions upstream [29, 30]. Hence, a plug flow reactor is used for each of the trailing parts to simulate a combustion process with low internal mixing. In addition, due to the contact of the two flames, a combined mixing flow is added to represent the mass transfer in between. An arrow pointing into the side of a reactor indicates that the flow is being added over a distance along the reactor to model a gradual as opposed to an instantaneous mixing process. Based on the average velocity flow field data from Dhanuka et al. [29], a parallel flow seems to exist around the overlapping region of the two flames. It is hence assumed that the net mass transfer between the two reactors through the combined mixing flow is zero, reducing one degree of freedom from the model. This system of two coupled plug flow reactors is termed a combined mixing plug flow reactor.

At the end of the combustor, the exhausts from the pilot and the main flames are gradually mixed into one stream [30], while the cooling air is introduced, which quickly slows down the chemical reaction rates [19]. Thus, a single ending PFR is used to first gradually merge the two streams into a homogeneous mixture and then

simulate the presence of cooling air. The outflow from the ending PFR then becomes the combustor exhaust.

2.3 Equations for Reactors

In this study, both well stirred reactors and plug flow reactors are used to construct the chemical reactor network. These two types of reactors solve two alternative simplified versions of the general conservation laws, which only involve solving ordinary differential equations. As a result, more computational power can be dedicated instead to detailed chemistry calculation to better resolve the emissions from the combustion process.

A well stirred reactor is a fixed control volume with an inlet and an outlet, containing a homogeneous mixture whose properties vary with respect to time [34]. On the other hand, a plug flow reactor is a fixed control volume with an inlet and an outlet, containing a heterogeneous mixture whose properties vary with respect to position [34]. In this section, the equations for a well stirred reactor and its variant, a non-uniform well stirred reactor, are presented first. Then, the equations for a plug flow reactor and its variant, a combined mixing plug flow reactor, are discussed.

2.3.1 Well Stirred Reactor

The well stirred reactor in this study has a constant volume, and the mixture within is spatially uniform. It resembles a reaction environment where diffusion is much faster than bulk flow, such that the mixture in any location within is instantaneously affected by changes in all other reactor locations. Three conservation equations are solved within a well stirred reactor, the conservation of mass, species, and energy [34]. The conservation of momentum equation is not explicitly solved in this reactor as a constant pressure is assumed within the combustor due to the typical low Mach number within. Because it is complicated and expensive to directly find a steady state solution [34], time-marching is used. Constant pressure is thus initially not enforced but gradually achieved by solving the system of equations repeatedly until reaching

steady state.

Equations for the conservation of mass are [34]:

$$\dot{m}_{\text{out}} = \dot{m}_{\text{in}} + K_{\text{v}} \cdot (P - P_{\text{comb}}) \tag{2.1}$$

$$P_{\text{comb}} = P_3 \cdot (1 - F_{\text{pres,loss}}) \tag{2.2}$$

$$\frac{dm}{dt} = \dot{m}_{\text{in}} - \dot{m}_{\text{out}} \tag{2.3}$$

P_{comb} is the static pressure to be preserved in this combustor, while P is the current time step static pressure within the reactor. K_{v} is a proportionality constant determining how strong the flow rate reacts to the pressure difference between P_{comb} and P. Thus, the second term on the right hand side of Equation 2.1 is a proportional controller enforcing the reactor internal pressure to be equal to the external pressure through time-marching [34]. K_{v} needs to be greater than 0 and a value of 1.0 $\text{m}\,\text{s}$ is used in this study. As shown by Equation 2.2, the combustor pressure P_{comb} is calculated based on the inlet pressure (P_3) and an estimated pressure loss fraction ($F_{\text{pres,loss}}$) due to the sudden expansion in the dome. Based on the influence coefficients in compressible flow, losses due to heat transfer are ignored as the Mach number is small. A constant $F_{\text{pres,loss}}$ is assumed to be 0.04 [35, 36]. Finally, Equation 2.3 calculates the mass differential term used to update the mass of the reactor mixture for the next time step.

The equation for the conservation of species is [34]:

$$\frac{dY_{\text{k}}}{dt} = \frac{\dot{\omega}_{\text{k}} \cdot W_{\text{k}}}{\rho} + \frac{\dot{m}_{\text{in}}}{m} \cdot (Y_{\text{k,in}} - Y_{\text{k}}) \tag{2.4}$$

The first term on the right hand side is the source term, the creation of species from chemical reactions. The $\dot{\omega}$ terms is the net production rate of species k calculated by Cantera [34] $\text{kmol}/(\text{m}^3\,\text{s})$. W_{k} is the molecular weight of species k, and ρ is the gas density. The second term on the right hand side is the species change caused

by inflow. There is no effect from the outflow because mass fraction is an intensive property. $Y_{\mathrm{k,in}}$ and Y_{k} are the mass fractions of species k in the inflow and within the reactor respectively.

Finally, the equation for the conservation of energy is [34]:

$$\frac{dT}{dt} = \frac{1}{m \cdot C_{\mathrm{p}}} \cdot \left[\dot{m}_{\mathrm{in}} \cdot \left(h_{\mathrm{in}} - \sum_{\mathrm{k=1}}^{\mathrm{n}} (h_{\mathrm{k}} \cdot Y_{\mathrm{k,in}}) \right) - \sum_{\mathrm{k=1}}^{\mathrm{n}} (h_{\mathrm{k}} \cdot \dot{\omega}_{\mathrm{k}} \cdot W_{\mathrm{k}} \cdot V) \right] \tag{2.5}$$

C_{p} is the constant pressure specific heat of the reactor mixture $\mathrm{J/(kg\,K)}$. h_{k} is the mass specific enthalpy of the species k within the reactor. h_{in} and $Y_{\mathrm{k,in}}$ are the mass specific enthalpy of the inflow and the mass fraction of the species k in the inflow. V is the reactor volume.

With the equations above, the non-linear ODE system for the well stirred reactor is formed with 2+n derivative terms, $\frac{dm}{dt}$, $\frac{dT}{dt}$, and $\frac{dY_{\mathrm{k}}}{dt}$, depending on 2+$n$ state variables, m, T, Y_{k} for $k = 1$ to n. This system is integrated in time until reaching steady state. Equilibrium condition of the inflow is used as the initial condition for the system to avoid converging to a trivial non-reacting solution [34]. Since radicals are consumed and created much faster than stable species, this ODE system is stiff [3]. Therefore, for each time step, a stiff ODE solver, VODE, is employed, whose backward differentiation schemes are capable of accurately resolving stiff problems [37]. The step size taken is determined by the solver automatically, while a maximum allowable time step Δt is specified to be 1% of the reactor residence time t_{res} for the purpose of saving intermediate results. To simulate a steady state solution, the total integration time t_{tot} is specified to be 10 times of the reactor residence time. The reactor residence time is estimated as:

$$t_{\mathrm{res}} \approx \frac{V \cdot \rho_{\mathrm{in}}}{\dot{m}_{\mathrm{in}}} \tag{2.6}$$

where ρ_{in} is the density of inflow.

2.3.2 Non-uniform Well Stirred Reactor

In the rich-burn region (primary zone) of a conventional RQL combustor, based on previous studies [32, 33], due to the separate injections and the non-perfect mixing of the fuel and air, multiple small and isolated hot pockets of combustible mixture, each with a distinct equivalence ratio, exist. Multiple well stirred reactors in parallel with different equivalence ratios were employed in this scenario [32, 33]. Since the pilot zone of a lean-burn staged combustor resembles the primary zone of an RQL combustor [12], these parallel reactors are also used in this study, as shown in Figure 2-3 [23].

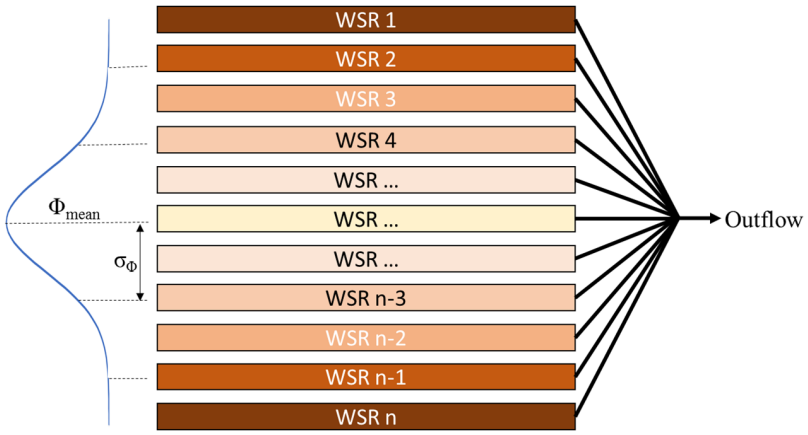

Figure 2-3: Non-uniform well stirred reactor

For simplicity, this thesis defines this kind of structure with parallel reactors as a "non-uniform well stirred reactor". The equivalence ratios of reactors are uniformly arranged around an average value, and then the air mass flow rates are normally distributed. The exact splitting procedure can be better explained using the equation [32, 23]:

$$\phi_{\text{mean}} = \frac{\dot{m}_1}{\dot{m}_2} \cdot \frac{1}{K_{\text{scale}}} \tag{2.7}$$

where $\dot{m}_1$ and $\dot{m}_2$ are the fuel and air flow rates, K_{scale} is the stoichiometric fuel air ratio FA_{st}, and ϕ_{mean} is an average equivalence ratio over all parallel reactors.

From Equation 2.8, as a normal distribution is employed, the standard deviation

σ_ϕ is calculated based on a mixing factor S_{mix}

$$\sigma_\phi = \phi_{\text{mean}} \cdot S_{\text{mix}} \tag{2.8}$$

that reflects on the level of heterogeneity of the mixture. For RQL combustors, it was shown to be acceptable to assume a constant mixing factor over different throttle conditions [32]. Thus, as a first order approximation, the same assumption is employed for the lean-burn staged combustor.

From Equations 2.9 to 2.12:

$$\Delta\phi = \frac{4 \cdot \sigma_\phi}{n-1} \tag{2.9}$$

$$\phi_{\text{min}} = \phi_{\text{mean}} - 2 \cdot \sigma_\phi \tag{2.10}$$

$$\phi_{\text{max}} = \phi_{\text{mean}} + 2 \cdot \sigma_\phi \tag{2.11}$$

$$\underline{\phi} = [\phi_{\text{min}}, \phi_{\text{min}} + \Delta\phi, \cdots, \phi_{\text{max}} - \Delta\phi, \phi_{\text{max}}] \tag{2.12}$$

a vector of equivalence ratios for the n reactors are generated ($\underline{\phi}$), linearly spanning between two standard deviations below and above the average value. Symbols with underlines are vector variables.

Then from Equations 2.13 and 2.14:

$$\underline{F_{\text{raw}}} = \frac{1}{\sigma_\phi \cdot \sqrt{2 \cdot \pi}} \cdot \exp \frac{-(\underline{\phi} - \phi_{\text{mean}})^2}{2 \cdot \sigma_\phi^2} \tag{2.13}$$

$$\underline{F} = \frac{\underline{F_{\text{raw}}}}{\sum \underline{F_{\text{raw}}}} \tag{2.14}$$

a corresponding vector of mass fractions $\underline{F}$ are computed and normalized, such that the total mass flow rate is conserved after the following step of splitting. All operations shown here are element-wise operations. There are also upper and lower limits set on the pilot flame equivalence ratio, which is from 0.189 to 3.600, and on the main

flame/SRF mass flow ratio, which is from 0.10 to 10.0. The main flame/SRF mass flow ratio is coded as an equivalence ratio by setting the stoichiometric fuel air ratio to unity. These limits are selected such that the non-uniform well stirred reactors produce non-trivial solutions when reaching steady state.

Stream two is first divided based on the mass fractions $\underline{F}$.

$$\underline{\dot{m}_2} = \dot{m}_2 \cdot \underline{F} \tag{2.15}$$

Then, stream one is distributed correspondingly based on the definition of ϕ.

$$\underline{\dot{m}_1} = \underline{\dot{m}_2} \cdot K_{\text{scale}} \cdot \underline{\phi} \tag{2.16}$$

After doing so, it can be verified that the mass flow rates for stream one and two are conserved.

The volumes are distributed assuming a constant pressure and residence time across the well stirred reactors.

$$\underline{V} = V \cdot \frac{\underline{\dot{m}_2} + \underline{\dot{m}_1}}{\underline{\rho}} \tag{2.17}$$

$\underline{\rho}$ is the vector of densities for the equilibrium states of the inflows to the well stirred reactors, which are calculated using Cantera [34] as:

$$\underline{\rho} = \frac{P_{\text{comb}} \cdot \underline{W}}{R_{\text{u}} \cdot \underline{T}} \tag{2.18}$$

where P_{comb} is the combustor constant pressure; R_{u} is the universal gas constant; $\underline{T}$ are the temperatures of the inflows after all the liquid phase substances, such as fuel, are vaporized and the equilibrium states are calculated; and $\underline{W}$ are the molecular weights of the inflows. The vaporization is calculated using Cantera [34] based on constant enthalpy and pressure. The idea of constant enthalpy is exemplified as:

$$\dot{m}_{\text{fuel}} \cdot (h^{\text{ini}}_{\text{fuel}} - H^{\text{v}}_{\text{fuel}}) + \dot{m}_{\text{air}} \cdot h^{\text{ini}}_{\text{air}} = (\dot{m}_{\text{fuel}} + \dot{m}_{\text{air}}) \cdot h^{\text{fin}}_{\text{mix}} \tag{2.19}$$

where h's are the mass specific enthalpies of gas phase species, and $H^{\text{v}}_{\text{fuel}}$ is the latent

heat of vaporization at the fuel initial temperature. In combustor model, fuel is assumed to be injected at the standard temperature of 298.15K, and Jet-A's latent heat of vaporization is assumed to be 358715 J/kg. To the end of the non-uniform well stirred reactor, all streams are combined instantaneously into a homogeneous exhaust stream.

2.3.3 Plug Flow Reactor

Similar to the well stirred reactor, the plug flow reactor in this study is under constant pressure and constant volume conditions. However, the flow within does not vary with respect to time but axial distance z [34]. This reactor represents a reaction environment where axial diffusion is negligible, such that the mixture upstream is completely unaffected by any change downstream. Mass, species, and energy conservation equations are solved in the reactor. The momentum equation is not employed due to the constant pressure assumption. In addition, mass flux is added along the length of the reactor to represent any potential mixing from adjoining reactors in the lateral direction.

For simplicity, it is assumed that there is no chemical reaction on the reactor wall, but only mass transfer exists. The mass flux β across the reactor wall is defined as follows in mass flow rate per unit distance [34].

$$\beta_{\text{wall,in}}(z) = \frac{\dot{m}_{\text{wall,in}}}{z_{\text{in,end}} - z_{\text{in,start}}} \qquad \text{for } z_{\text{in,start}} <= z <= z_{\text{in,end}} \tag{2.20}$$

$$\beta_{\text{wall,out}}(z) = \frac{\dot{m}_{\text{wall,out}}}{z_{\text{out,end}} - z_{\text{out,start}}} \qquad \text{for } z_{\text{out,start}} <= z <= z_{\text{out,end}} \tag{2.21}$$

$\dot{m}_{\text{wall}}$ is the total mass flow rate in or out of the reactor wall. z_{start} and z_{end} are the corresponding starting and ending z position along the reactor where the inlet/outlet

mass flux occurs. The conservation equations for mass, species, and energy are then:

$$\frac{d\dot{m}}{dz} = \beta_{\text{wall,in}} - \beta_{\text{wall,out}} \tag{2.22}$$

$$\frac{dY_{\text{k}}}{dz} = \frac{\beta_{\text{wall,in}}}{u \cdot A \cdot \rho} \cdot (Y_{\text{k,wall,in}} - Y_{\text{k}}) + \frac{\dot{\omega}_{\text{k}} \cdot W_{\text{k}}}{u \cdot \rho} \tag{2.23}$$

$$\frac{dT}{dz} = \frac{1}{\dot{m} \cdot C_{\text{p}}} \cdot \left[\beta_{\text{wall,in}} \cdot \left(h_{\text{wall,in}} - \sum_{\text{k=1}}^{\text{n}} (h_{\text{k}} \cdot Y_{\text{k,wall,in}}) \right) - A \cdot \sum_{\text{k=1}}^{\text{n}} (\dot{\omega}_{\text{k}} \cdot W_{\text{k}} \cdot h_{\text{k}}) \right] \tag{2.24}$$

All variables with the subscript "wall" are properties for the side flow, while those without are properties for the reactor internal flow at the current location z. As the species k mass fraction Y_{k} and the mixture temperature T are intensive properties, side flow out does not have an effect on them and thus does not appear in the equations. For the species equation, $\dot{m}$ is decomposed into three parts: axial flow velocity u, constant reactor cross-sectional area A, and internal flow density ρ. $\dot{\omega}_{\text{k}}$ is the net production rate for species k calculated by Cantera [34], and W_{k} is the molecular weight of species k. C_{p} is the constant pressure specific heat of the mixture, and h is the corresponding mass specific enthalpy.

To fully characterize the reactor, the following parameters are also defined.

$$\Delta Z_{\beta} = \frac{z_{\text{wall,end}} - z_{\text{wall,start}}}{L} \tag{2.25}$$

$$V = A \cdot L \tag{2.26}$$

L and ΔZ_{β} are the total length of the reactor and the fraction of length along which flow is crossing the wall. In addition, either the starting $z_{\text{wall,start}}$ or the ending $z_{\text{wall,end}}$ boundary must be specified to locate the side flow. A constant cross-sectional area is assumed for a reactor.

For the same reason as in the well stirred reactor, the VODE ODE solver is

employed to solve the plug flow reactor. The solution is computed from the starting z to the ending z location of the reactor with a maximum allowable step size Δz equal to 1% of the total reactor length L.

2.3.4 Combined Mixing Plug Flow Reactor

A combined mixing plug flow reactor is a set of two coupled plug flow reactors with the side flow crossing from one reactor into the other reactor and vice versa. It is used to model the mixing between two streams over a distance. An illustration is shown in Figure 2-4, where the subscript "wall" for side flow is omitted for better readability.

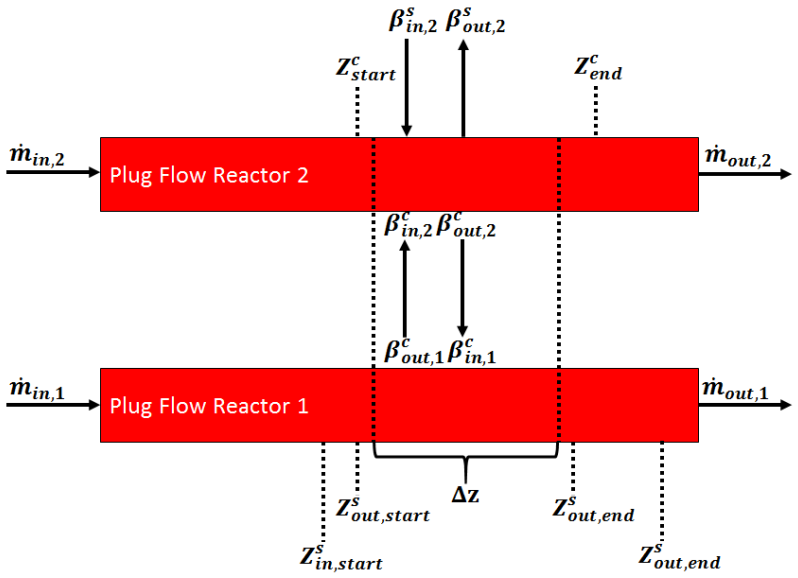

Figure 2-4: Combined mixing plug flow reactor

Besides the inlets and outlets to the plug flow reactors, shown here are the side flows modeled for one Δz step. Treating these coupled reactors as one system, side flow can be classified into two types, a "specified side flow" with superscript 's' communicating between the system and the outside environment, and a "combined mixing side flow" with superscript 'c' between the two coupled reactors. The properties of side flows are updated in every Δz depending on the current z location, where Δz is the maximum allowable distance step for the VODE solver. The definition of mass flux is:

$$\beta_{\text{wall}} = \begin{cases} \frac{\dot{m}_{\text{wall}}}{z_{\text{wall,end}} - z_{\text{wall,start}}} & \text{if } z_{\text{wall,start}} <= z <= z_{\text{wall,end}} \\ 0 & \text{otherwise} \end{cases} \tag{2.27}$$

This definition is applied over the four side flow zones, which are the "combined mixing inflow zone", "combined mixing outflow zone", "specified inflow zone", and the "specified outflow zone". Each zone is characterized by a total flow rate and two boundaries, $\dot{m}$, z_{start}, and z_{end}. For the specified side flow, z_{start} and z_{end} can be defined arbitrarily; however, for the combined mixing side flow, the outflow zone for one reactor must match with the inflow zone for the other reactor to conserve mass. Constant β is assumed within each zone for simplicity, while the side flow temperature and compositions might vary from step to step depending on the reactor internal flow.

2.3.5 Reaction Mechanism and Jet Fuel Surrogate

When calculating the chemistry source term in the species conservation equation, the "high temperature C0-C16" CRECK reaction mechanism [38, 39] is used along with Cantera [34]. The CRECK mechanism simulates the oxidation of a wide range of hydrocarbon fuels and the formation of PAH species. Then, the CRECK mechanism is further combined with a NO_x reaction mechanism [40, 41, 42] to compute the NO_x emissions. The NO_x mechanism used here operates on both high and low temperature regimes and simulates all thermal NO_x, prompt NO_x, and N_2O-intermediate NO_x reactions. Moreover, in order to accurately capture the thermal and chemical properties of Jet-A, a surrogate [2] with its composition shown in Table 2.1 is selected.

Table 2.1: Jet fuel surrogate [2].

Species	Mole Fraction
n-Dodecane	0.3706
Iso-Octane	0.0195
Toluene	0.2591
Iso-cetane	0.2059
Decalin	0.1449

2.4 Operation and Calibration of the Combustor Model

Before using the combustor model to predict NO_x emissions at different engine conditions, the design parameters of the chemical reactor network need to be first calibrated for the model to be realistic. This section starts by discussing the operation of the combustor model across different engine throttle conditions. Then, the calibration process is explained with all design parameters summarized.

2.4.1 Operation

At each engine throttle condition, the inputs to the chemical reactor network are the inlet air flow rate $\dot{m}_{\text{air},3}$, fuel flow rate $\dot{m}_{\text{fuel},3}$, temperature T_3, and pressure P_3. All the fuel is injected into the dome region of the combustor, which corresponds to the main root WSR and the pilot root WSR from Figure 2-2. T_3 is the temperature of the air flowing into the two WSRs, while P_3 multiplied by a viscous loss factor as discussed previously is the constant pressure held by all reactors.

The distribution of total fuel flow over the two WSRs depends on the staging conditions, characterized by a fuel split ratio S_{fuel} and a main zone staging equivalence ratio $\phi_{\text{main,switch}}$ as:

$$\phi_{\text{main}} = \frac{\dot{m}_{\text{fuel,main}}}{\dot{m}_{\text{air,main}} \cdot FA_{\text{st}}} \tag{2.28}$$

$$S_{\text{fuel}} = \frac{\dot{m}_{\text{fuel,main}}}{\dot{m}_{\text{fuel,pilot}}} \tag{2.29}$$

$$\dot{m}_{\text{fuel,pilot}} = \begin{cases} \frac{\dot{m}_{\text{fuel},3}}{1+S_{\text{fuel}}} & \text{if } \phi_{\text{main}} > \phi_{\text{main,switch}} \\ \dot{m}_{\text{fuel},3} & \text{otherwise} \end{cases} \tag{2.30}$$

$$\dot{m}_{\text{fuel,main}} = \begin{cases} \dot{m}_{\text{fuel},3} - \dot{m}_{\text{fuel,pilot}} & \text{if } \phi_{\text{main}} > \phi_{\text{main,switch}} \\ 0 & \text{otherwise} \end{cases} \tag{2.31}$$

FA_{st} is the stoichiometric fuel air ratio, and ϕ_{main} is the equivalence ratio of the

main root WSR. $\phi_{\text{main,switch}}$ is chosen to be the threshold for staging to ensure a stable main flame. The calculations above are coupled and thus need to be performed in the following order. The S_{fuel} and $\dot{m}_{\text{fuel,3}}$ are first used to calculate a tentative $\dot{m}_{\text{fuel,main}}$ and ϕ_{main} assuming the main-also operation mode. Then, the tentative ϕ_{main} can be used to determine whether a stable main flame can be sustained or the $\dot{m}_{\text{fuel,main}}$ needs to be recalculated under the pilot-only mode instead.

In terms of the fuel distribution, a constant S_{fuel} is assumed. This is the simplest splitting strategy assuming the main fuel injectors have only two states (on/off). Therefore, at each throttle condition in main-also mode, the fuel split ratio between the injectors is fixed.

The total air flow $\dot{m}_{\text{air,3}}$ is distributed to the main root WSR, pilot root WSR, and ending PFR as shown in Figure 2-2. The distribution is based on the air split fractions $F_{\dot{\text{m}}}$ defined as:

$$\dot{m}_{\text{air,main}} = F_{\dot{\text{m}},\text{air,main}} \cdot \dot{m}_{\text{air,3}} \tag{2.32}$$

$$\dot{m}_{\text{air,pilot}} = F_{\dot{\text{m}},\text{air,pilot}} \cdot \dot{m}_{\text{air,3}} \tag{2.33}$$

$$\dot{m}_{\text{air,end}} = \dot{m}_{\text{air,3}} - \dot{m}_{\text{air,main}} - \dot{m}_{\text{air,pilot}} \tag{2.34}$$

For an RQL combustor, a constant air distribution over different throttle conditions was previously adopted [23] successfully to study engine emissions. Thus, as a first approximation, constant combustor air split fractions are also employed for this staged combustor model. Although a reduction in the main zone air flow rate when increasing the main zone fuel flow rate was observed previously [18], the exact amount of air flow reduction at different thrust level is still unclear, and whether this phenomenon is common for the lean-burn staged combustor is uncertain.

Given the assumptions on air and fuel distributions above, the equivalence ratio evolutions for the two WSRs are shown in Figure 2-5. Staging occurs when the main zone equivalence ratio is above the threshold $\phi_{\text{main,switch}}$ which is 0.4 in this case. For

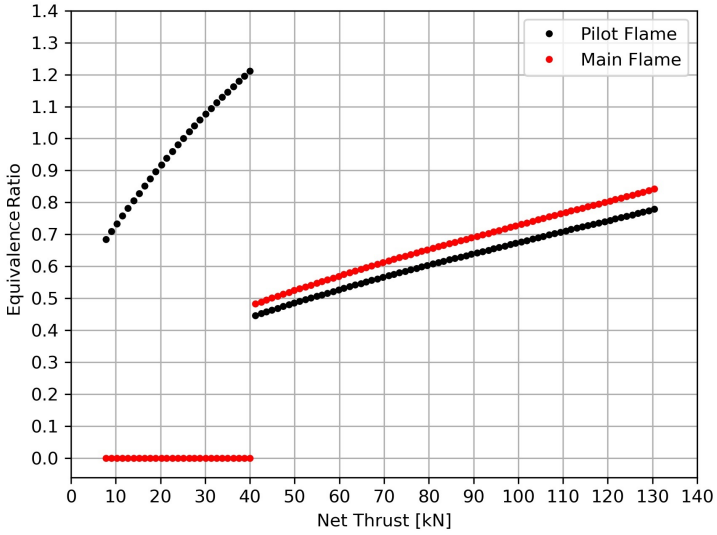

Figure 2-5: Dome equivalence ratio evolution

pilot-only operation, fuel is only injected into the pilot flame and thus creates mostly a rich-burn condition to enhance combustion stability. However, during main-also operation, fuel is distributed such that both flames are burning lean to achieve low NO_x emissions.

Because the air split fraction is not an intuitive design parameter that gives a direct indication of whether the combustor is operating in a rich-burn or lean-burn condition, the air split fractions are replaced by two alternative design parameters $\phi_{\text{main,des}}$ and $\phi_{\text{pilot,des}}$, which are the combustor design point equivalence ratios for the main root WSR and the pilot root WSR. The design point of the combustor is usually picked as the maximum power condition, corresponding to the 100% rated thrust from Figure 2-5. In Figure 2-5, $\phi_{\text{main,des}}$ and $\phi_{\text{pilot,des}}$ are 0.65 and 0.76 respectively. The constant air split fractions are in turn determined using:

$$F_{\dot{m},\text{air,main}} = \frac{\dot{m}_{\text{fuel,main,des}}}{\phi_{\text{main,des}} \cdot FA_{\text{st}} \cdot \dot{m}_{\text{air,3}}} \tag{2.35}$$

$$F_{\dot{m},\text{air,pilot}} = \frac{\dot{m}_{\text{fuel,pilot,des}}}{\phi_{\text{pilot,des}} \cdot FA_{\text{st}} \cdot \dot{m}_{\text{air,3}}} \tag{2.36}$$

where $\dot{m}_{\text{fuel,main,des}}$ and $\dot{m}_{\text{fuel,pilot,des}}$ are the design point fuel flow rates to the two flames calculated using the constant fuel split ratio S_{fuel} defined previously.

It has been shown by previous studies based on CFD results and PLIF measurements that different fuel distributions do not have a strong effect on the total flow structure [18], and that the presence of the main flame does not have much effect on the position of the pilot flame [29]. Both observations indicate a relatively steady flow structure within a lean-burn staged combustor. Therefore, it is assumed that the general layout of the chemical reactor network and the volume of each reactor are unchanged across different operating points.

The step recirculation flow $\dot{m}_{\text{SRF}}$ and the combined mixing flow $\dot{m}_{\text{comb,mix}}$ are also distributed based on the splitting fractions $F_{\dot{m}}$, defined as:

$$\dot{m}_{\text{SRF}} = (\dot{m}_{\text{fuel,pilot}} + \dot{m}_{\text{air,pilot}}) \cdot F_{\dot{m},\text{SRF}} \tag{2.37}$$

$$\dot{m}_{\text{comb,mix}} = \frac{\dot{m}_{\text{exhaust,pilot,root}} + \dot{m}_{\text{exhaust,main,root}}}{2} \cdot F_{\dot{m},\text{comb,mix}} \tag{2.38}$$

The idea behind this is that a higher flow rate tends to induce stronger mixing between streams, and it is assumed that the level of mixing is directly proportional to the flow rate. The $\dot{m}_{\text{exhaust}}$ is the mass flow rate of exhaust. For combined mixing, as the mass transfer is bidirectional, the fraction is thus based on the average flow rate of the two streams. As mentioned previously, the net flow rate between the two PFRs in combined mixing is assumed to be 0. Thus, this $\dot{m}_{\text{comb,mix}}$ is both the $\dot{m}_{\text{in,comb,mix}}$ and $\dot{m}_{\text{out,comb,mix}}$ for each PFR.

The fraction of PFR length along which combined mixing side flow occurs is characterized by $\Delta Z_{\beta,\text{comb,mix}}$. Similarly, $\Delta Z_{\beta,\text{end,join}}$ and $\Delta Z_{\beta,\text{end,cool}}$ are used to define the two side flow zones on the ending PFR where the exhausts from the combined mixing PFR mix into a homogeneous mixture and where the cooling flow quenches into the ending PFR.

To fully specify the three side flow zones mentioned above, for the combined mixing and the end-join flow, it is assumed that both zones start at the beginning

of the reactors, meaning $z_{\text{comb,mix,start}} = z_{\text{end,join,start}} = 0$. For the cooling flow, the zone terminates by the end of the reactor, meaning $z_{\text{cool,end}} = L_{\text{end}}$. These parameters are predetermined to reduce the unnecessary degrees of freedom for the model. With all the operation related parameters defined in this section, the model can then be calibrated to represent a realistic engine combustor.

2.4.2 Calibration

The ICAO Aircraft Engine Emissions Databank (EEDB) collects the experimentally measured emissions data for all certified aircraft engines provided by their manufacturers [1]. Emissions data are measured at sea level static (SLS) conditions, operating at four throttle conditions corresponding to the Landing-Takeoff Cycle (LTO), including takeoff (100% rated thrust), climb-out (85% rated thrust), approach (30% rated thrust), and idle (7% rated thrust). The emissions data are then corrected to the International Standard Atmosphere (ISA) conditions with an additional humidity correction [43]. Thus, with a certain set of design parameters, if the combustor model running at the same SLS, LTO, and ISA conditions can reproduce the experimentally-measured emissions data from the EEDB, it indicates that the design parameters are well calibrated and validated, and the model represents a real combustor to a certain extent.

After the calibration, the model can then be operated at conditions other than SLS, LTO, and ISA to estimate engine emissions in scenarios where experimental data are currently lacking. More importantly, the calibrated model parameters can later be perturbed to study the sensitives of emissions on different combustor design variables, which would potentially give insights into more advanced future combustor development.

The pollutants to be calibrated against and studied in this work are the emission indices of NO_x and CO. The LEAP-1B combustor LTO emissions data from EEDB are shown in the Figure 2-6 [1]. These data are for multiple LEAP-1B engines with different rated thrusts. Therefore, if normalizing the thrust levels of all these engines with respect to the maximum rated thrust, the LTO cycle then corresponds to not

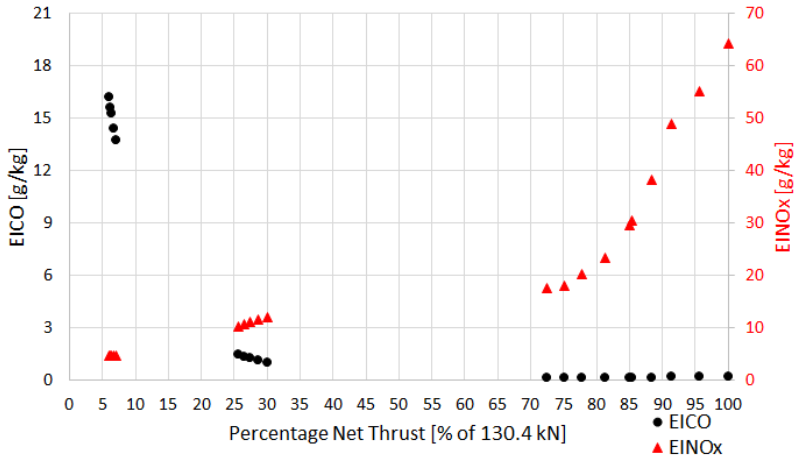

Figure 2-6: LEAP-1B LTO emissions data from EEDB [1]

just four distinct thrust levels but four different ranges of thrust levels. In Figure 2-6, thrust levels are takeoff (100%-85% rated thrust), climb-out (85%-72% rated thrust), approach (30%-25% rated thrust), and idle (7%-6% rated thrust). Considering the computational cost of evaluating the combustor model, usually a subset of data points are selected from the EEDB data for the calibration of the combustor model design parameters.

Table 2.2 summarizes all the design parameters for the combustor model. The variables are classified into "calibrated parameters" and "predetermined parameters". The air fractions are actually shown as opposed to the design point equivalence ratios as mentioned previously, because providing calibrated air fractions in this work helps future studies reproduce current results, though equivalence ratios are the actual design parameters calibrated.

The "calibrated parameters" are varied such that the model calculated emissions match with the EEDB data. The "predetermined parameters" are selected based on the following three criteria: (1) that they don't have significant impacts on the emissions of the target pollutants, (2) their effects can be replaced by other parameters, (3) or well educated guesses of their values can be made based on previous studies.

Among the predetermined parameters, all the lengths of the plug flow reactors do not impact the emissions because the residence time depends instead on the volume

Table 2.2: Combustor model design parameters.

Calibrated Parameters	Symbol	Predetermined Parameters	Symbol	Value
Fuel Split Ratio	S_{fuel}	Staging Equivalence Ratio	$\phi_{\text{main,switch}}$	Auto
Pilot Root Air Fraction	$F_{\dot{m},\text{pilot}}$	End-Join Length Fraction	$F_{\text{len,end,join}}$	0.3
Main Root Air Fraction	$F_{\dot{m},\text{main}}$	Comb-Mix Length Fraction	$F_{\text{len,comb,mix}}$	1.0
Pilot Root Mixing Factor	$S_{\text{mix,pilot}}$	Number of Pilot sub-WSRs	n_{pilot}	21
Main Root Mixing Factor	$S_{\text{mix,main}}$	Number of Main sub-WSRs	n_{main}	21
SRF Mass Fraction	$F_{\dot{m},\text{SRF}}$	Pilot Tail Length	$L_{\text{pilot,tail}}$	0.035
Comb-Mix Mass Fraction	$F_{\dot{m},\text{comb,mix}}$	Main Tail Length	$L_{\text{main,tail}}$	0.035
End-Cool Length Fraction	$F_{\text{len,end,cool}}$	Ending Length	L_{end}	0.035
Pilot Root Volume	$V_{\text{pilot,root}}$			
Main Root Volume	$V_{\text{main,root}}$			
Pilot Tail Volume	$V_{\text{pilot,tail}}$			
Main Tail Volume	$V_{\text{main,tail}}$			
Ending Volume	V_{end}			

of the reactor, and the length is only an artifact of the equation derivation. The choice of the number of reactors is based on the computational cost of evaluating the combustor model. The fraction of length for combined mixing is a redundant variable as its effects can be emulated by the reactor volume and the mass flow rate. The fraction of length for the end-join side flow zone is also an insignificant variable based on preliminary test results. For only the calibration purpose, the main zone staging threshold is automatically set to an equivalence ratio corresponding to the cruise operation, because the calibration thrust levels are only from the LTO cycle.

From Table 2.2, it is observed that even after excluding the predetermined parameters, there are still 13 parameters to be calibrated. The calibration is thus difficult without an initial guess in the vicinity of the targeted solution. Therefore, the influence of each calibrated parameter is first evaluated numerically and then used to set a preliminary state close to the target solution.

Based on preliminary tests, it is found that there exist many local minima in the objective field, and a gradient based method, such as the conjugate gradient algorithm, tends to converge to a local optimal solution and then stop. Therefore, once a feasible initial guess of the design parameters is determined, later calibration is carried out by the non-gradient based DIRECT algorithm from SciPy [44, 45], which balances the search between the global and the local solutions and is able to quickly shrink the search zones around minima in the objective field.

2.5 Combustor Inlet Conditions

Although the ICAO Aircraft EEDB provides the fuel flow rates for all thrust conditions and the bypass ratios and overall pressure ratios for all the rated thrust levels, an engine cycle model is still needed to convert this information into combustor input variables, which are the inlet air flow rate $\dot{m}_{\text{air},3}$, fuel flow rate $\dot{m}_{\text{fuel},3}$, temperature T_3, and pressure P_3. After calibrating the combustor, an example flight mission is used to predict the cruise emissions performance of the engine.

This section first discusses an example flight mission created from the Transport Aircraft System OPTimization model (TASOPT) [46]. Then, an engine cycle model developed on the Numerical Propulsion System Simulation (NPSS) thermodynamic modeling environment [47] is presented, which satisfies the thrust requirements from TASOPT.

2.5.1 Example Flight Mission

TASOPT [46] is an aircraft-engine-mission design optimizer considering multiple structural, aerodynamic, and power constraints. It primarily utilizes fundamental governing equations to model different aspects of the aircraft. Hence, TASOPT is employed to generate a representative flight mission for this study.

Because lean-burn staged combustors are the main interest of this study, the engine models used in this thesis approximate the performance of a LEAP-1B engine on a Boeing 737MAX aircraft. However, due to the lack of publicly available performance data for these two products and the various approximations made in this study, the models shown here only reflect their real-life counter parts to a certain degree.

The fight mission was constructed from multiple sources by Prakash [48]. A Boeing 737-800 aircraft model from TASOPT was first used as a baseline [49]. Then, modifications to the payload and engine are made using information from Brady [50]. The model gives a reasonable estimation of the drag and thrust requirements of a semi-realistic aircraft on a design mission. The flight mission parameters are shown in Figure 2-7.

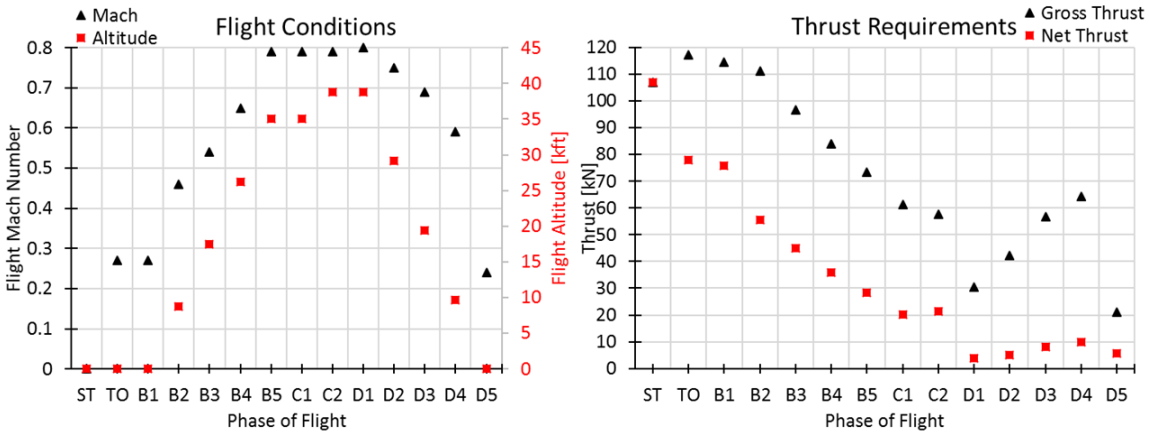

Abbreviation	ST	TO	B	C	D
Description	Static	Takeoff	Climb-out	Cruise	Descent

Figure 2-7: TASOPT flight mission parameters

The static phase is a sea level static rated thrust operation. Takeoff and initial climb-out are modeled at sea level conditions. Two cruise conditions are modeled to represent the start and end of cruise. On the right of the figure, the difference between the gross thrust and net thrust is the engine ram drag induced by a non-zero inflow momentum, which increases as the flight velocity increases.

Among all the flight phases from Figure 2-7, the top of climb condition (B5) is the most demanding one due to the high thrust requirement and the low air density. Hence, on top of those LTO thrust conditions from the EEDB, the NPSS engine cycle model presented in the next section must satisfy this B5 thrust requirement for it to be capable of performing all other phases.

2.5.2 Engine Cycle Model

NPSS [47] is a thermodynamic cycle modeling environment capable of simulating the performance of an aircraft engine. It is employed to create a turbofan engine model resembling the LEAP-1B engine for the emissions analysis of this thesis. The general flow structure of the turbofan model is shown in Figure 2-8.

One notable feature of this model is the parallel arrangement of the fan and low pressure compressor (LPC). This is because the fan root is modeled as a part of the

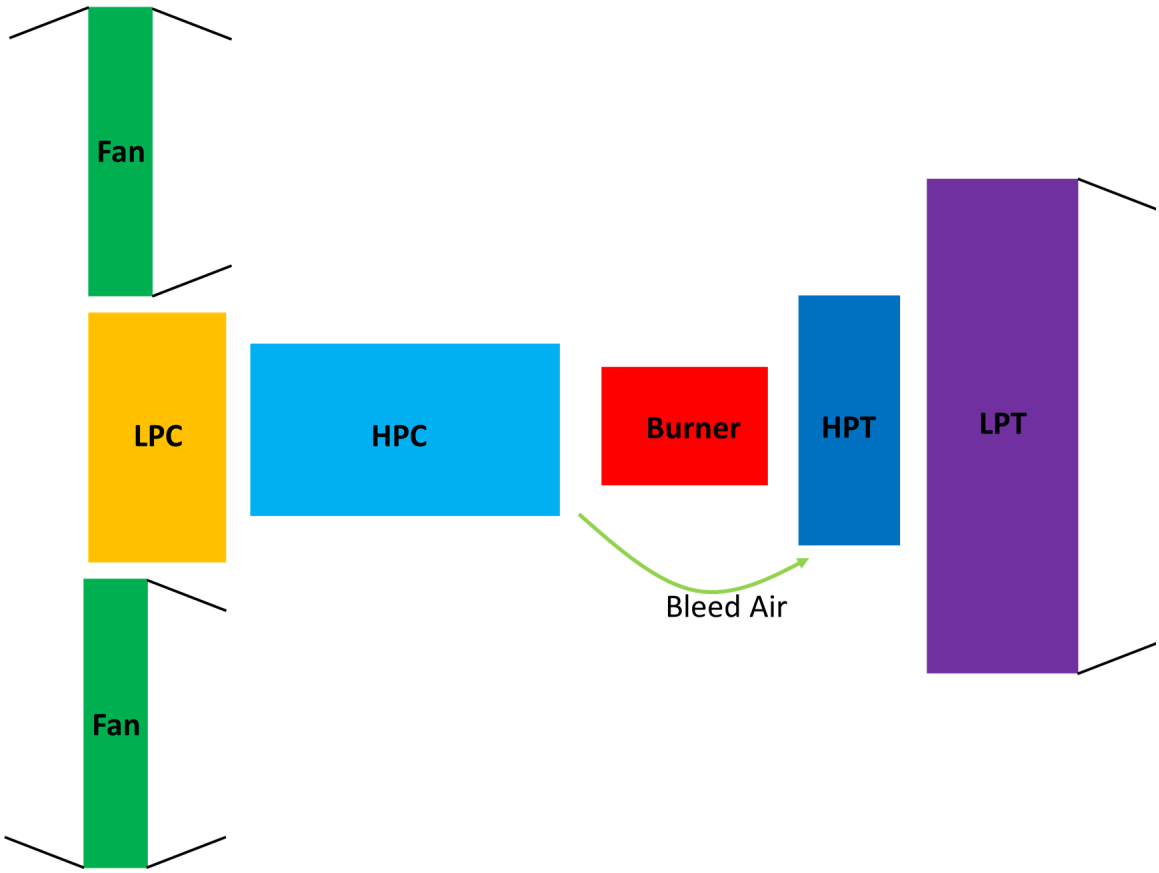

Figure 2-8: NPSS two-spool turbofan engine model

LPC rather than the fan and thus shares the same compressor map of the LPC, while the fan map is only used for the portion going to the bypass flow. Separated and conical nozzles are used, similar to those on the LEAP-1B engine, and the low pressure turbine directly drives the LPC and the fan.

With the general flow structure created, the engine cycle calibration is performed with the procedure shown in Figure 2-9. Top of climb is used as the engine sizing point, while all the EEDB data points are used as the off-design points. For the fixed parameters, the thrust F_n, altitude Alt_{amb}, ambient Mach number Ma_{amb}, and ambient humidity Hum_{amb} are all known parameters from the TASOPT mission and EEDB data from the previous section. The $Ma_{internal}$ are the sizing point Mach numbers in all the internal channels of the engine that are picked based on typical values and are later used to size the channels cross-sectional areas. The sizing point outlet pressure P_{outlet} is the ambient pressure at altitude that is used to size the

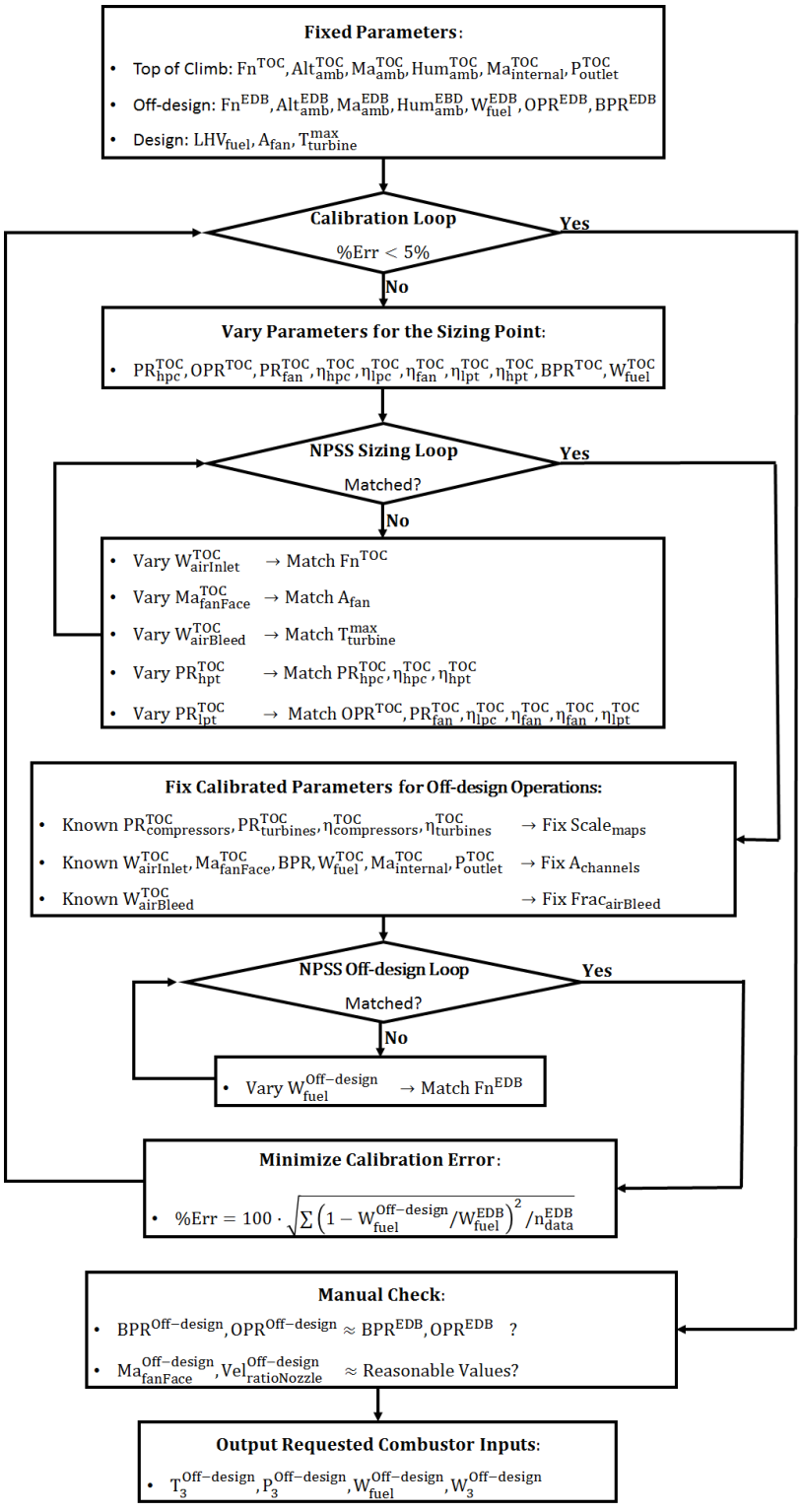

Figure 2-9: NPSS calibration procedure

nozzle, assuming isentropic expansion. The turbine maximum temperatures are set to typical turbine temperature limits, 2200 R for stators and 2000 R for rotors, to size the bleed air fraction. The area of the fan is calculated based on a known fan diameter d_{fan} = 78 in and a measured fan hub-to-tip ratio R_{ht} = 0.27 as:

$$A_{fan} = (\frac{d_{fan}}{2})^2 \cdot \pi \cdot (1 - R_{ht}^2) \tag{2.39}$$

The area of the fan here includes the fan root region. Typical Jet-A fuel is used with a heating value of LHV_{fuel} = 43.27 MJ/kg as indicated in the EEDB [1].

Chapter 3

Results

This section starts with the calibration of the combustor model and the NPSS engine cycle model. Alternative calibrated models are presented along with the reasons why they are not selected. Then, at the sea-level static conditions, NO_x emissions from the lean-burn staged combustor are analyzed, followed by an analysis of emissions during a representative flight mission. After that, the effects of varying the fuel split ratio on NO_x emissions are presented in detail. This section ends with a comparison of the NO_x emission performance of an RQL combustor against a lean-burn staged combustor, with both combustor models running on the same engine cycle.

3.1 Engine Model Validation

An engine model is calibrated against the LEAP-1B EEDB results as shown in Figure 3-1, 3-2, and 3-3. The relative RMS errors for fuel flow rate, overall pressure ratio, and bypass ratio are 0.75%, 1.45%, and 0.79%, respectively. The exhaust velocity ratios of bypass over core flow are between 0.6 and 1.0 during cruise, takeoff, and climb-out phases. Fan face Mach numbers at cruise are between 0.6 and 0.65. These values are consistent with those of a typical gas turbine engine, indicating that the engine model used in this study is realistic.

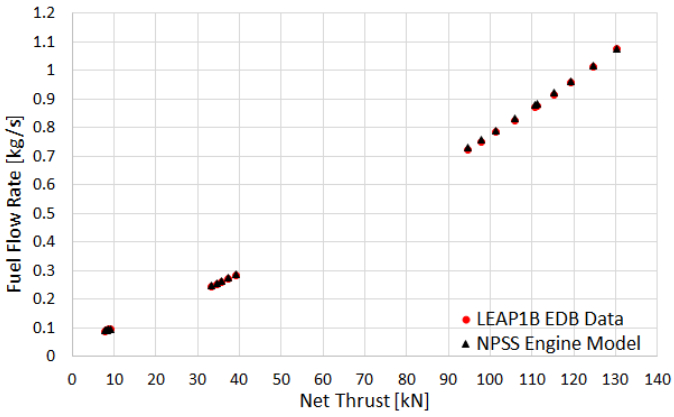

Figure 3-1: Fuel flow rate validation for NPSS engine cycle model

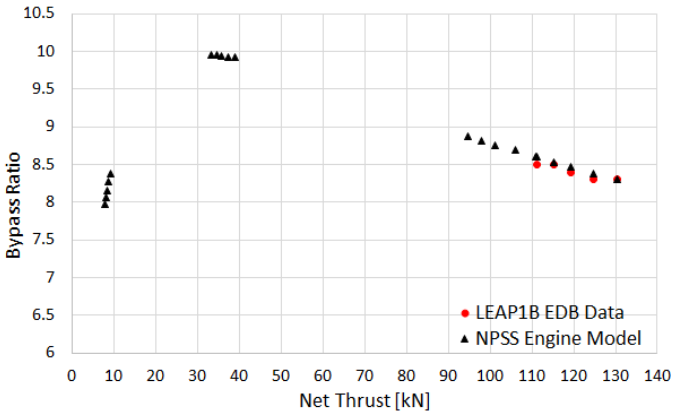

Figure 3-2: Bypass ratio validation for NPSS engine cycle model

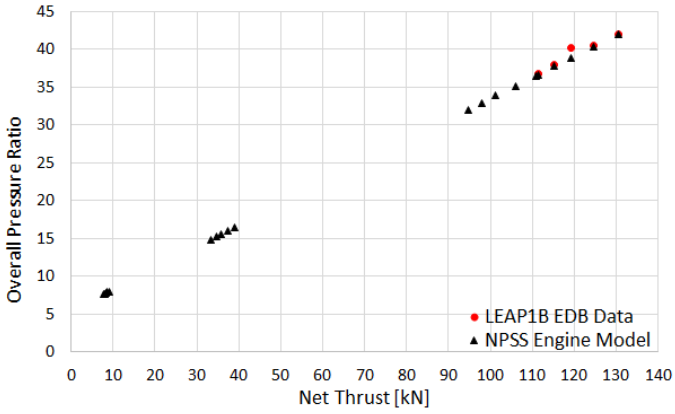

Figure 3-3: Overall pressure ratio validation for NPSS engine cycle model

3.2 Combutor Model Validation

After the calibration of the NPSS engine cycle model, burner inlet conditions from NPSS at the thrust levels presented in EEDB and their corresponding NO_x and CO

emission data points are then used to calibrate the combustor model. For the lean-burn staged combustor, a comparison between the EEDB EI_{NO_x} and EI_{CO} for the LEAP-1B engine and the model-predicted emission levels are shown in Figures 3-4 and 3-5 respectively.

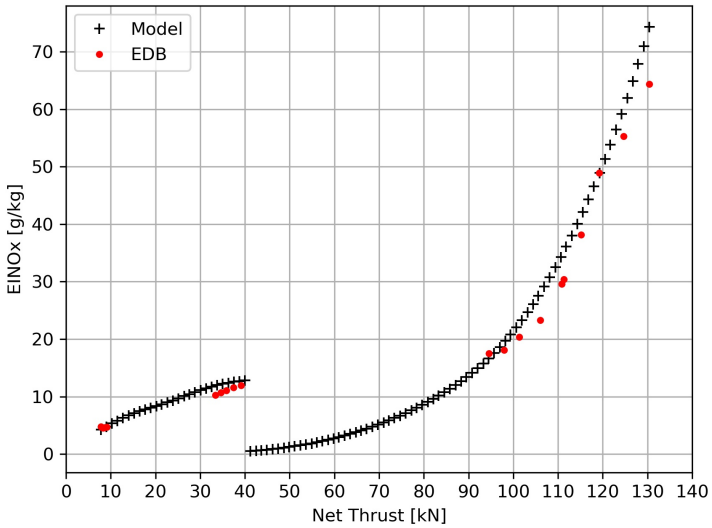

Figure 3-4: Validation of EI_{NO_x} for the lean-burn staged combustor

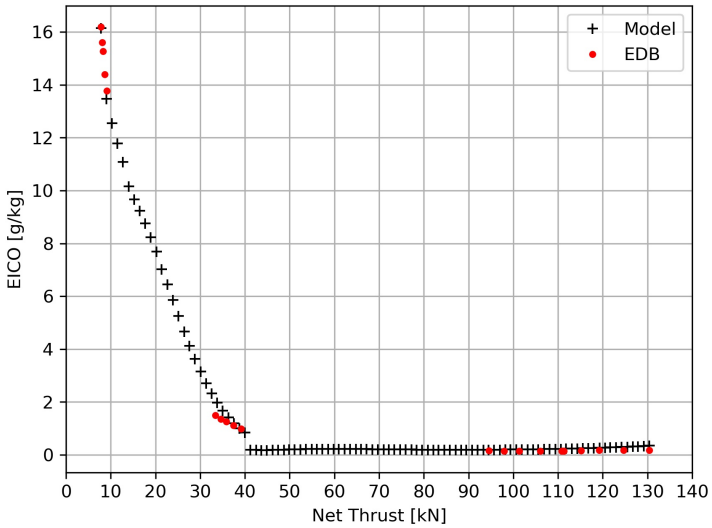

Figure 3-5: Validation of EI_{CO} for the lean-burn staged combustor

The relative RMS errors for NO_x and CO are 2.7% and 0.73% respectively. As

mentioned previously, the process of turning on the main fuel injector when switching from low power to high power operation is termed "staging" in this thesis. In this calibrated combustor model, "staging" is assumed to occur at the thrust of 40 kN which corresponds to a 30% rated thrust or the approach phase condition. Staging causes the NO_x emissions to decrease to 0.5 g/kg. For the high power operation, the EI_{NO_x} EEDB data points follow two different trends with which the model-predicted results are not matching perfectly. However, one potential hypothesis for these two-trend EI_{NO_x} EEDB data points is discussed in Section 3.6.

The calibrated burner parameters are shown in Table 3.1.

Table 3.1: Calibrated design parameters for the lean-burn staged combustor model.

Calibrated Parameters	Value	Predetermined Parameters	Value
Fuel Split Ratio	1.75	Staging Equivalence Ratio	0.48
Pilot Root Air Fraction	19%	End-Join Length Fraction	30%
Main Root Air Fraction	31%	Comb-Mix Length Fraction	100%
Pilot Root Mixing Factor	85%	Number of Pilot sub-WSRs	21
Main Root Mixing Factor	0.0%	Number of Main sub-WSRs	1
SRF Mass Fraction	0.0%	Pilot Tail Length	3.5 cm
Comb-Mix Mass Fraction	38.0%	Main Tail Length	3.5 cm
End-Cool Length Fraction	55%	Ending Length	3.5 cm
Pilot Root Volume	220 cm^3		
Main Root Volume	700 cm^3		
Pilot Tail Volume	430 cm^3		
Main Tail Volume	200 cm^3		
Ending Volume	2300 cm^3		

Among the predetermined parameters, the staging equivalence ratio is eventually selected such that the combustor staging occurs when the throttle is right above the approach phase thrust requirement. This corresponds to the lowest possible staging thrust threshold as can be observed from the EEDB data points. The number of main sub-WSRs is reduced to 1 as the calibration process indicates that the stabilizing effect from the stage recirculation flow cannot be modeled accurately by the current reactor network. Hence, from calibrated parameters, the SRF mass fraction and the main root mixing factor are eventually set to 0%, which means the main zone mixture is completely homogeneous. Based on the air fractions, it is indicated that 50% of combustor air is eventually used for cooling. Although this is not consistent with the

30% cooling air indicated by the FAA CLEEN program final report [12], the report did not actually indicate whether the combustor is specifically for LEAP-1A or -1B engine, so it is still plausible that a 50% cooling air is realistic for the current model.

A fuel split ratio of 1.75 is selected, which corresponds to 36% of the total fuel being injected through the pilot fuel injector. The corresponding evolution of the pilot flame and main flame equivalence ratios is shown in Figure 2-5.

Because the main flame is modeled as a premixed flame, it performs a lean-burn process throughout the range of operation with its equivalence ratio varying from 0.5 to 0.85. This lean flame keeps the NO_x production level low until the equivalence ratio approaches one. On the other hand, although it seems that during high power operation the pilot flame is leaner than the main flame from Figure 2-5, because of its non-premixed property, its equivalence ratio actually approaches unity locally through most part of the operation. This phenomenon is observed in Figure 3-6.

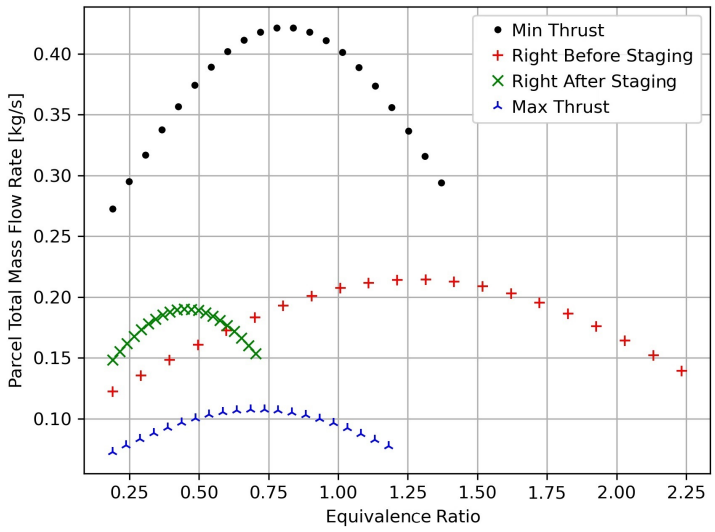

Figure 3-6: Pilot flame equivalence ratio evolution

Figure 3-6 shows the distribution of equivalence ratios across the multiple pilot root sub-WSRs on four throttle conditions of interest. Those right before staging and right after staging cases are the conditions at 40 kN thrust from Figure 2-5. As there are 21 sub-WSRs for the pilot root, each operating condition consists of 21 data

points. Each point has a unique local equivalence ratio and mass flow rate. The air flow rates are normally distributed about the mean equivalence ratio, while the fuel flow rates are directly calculated from the air flow rates. Therefore, the total mass flow rates are not completely symmetric.

What can also be observed from the minimum thrust case up to the staging point is that the pilot flame contains a stoichiometric region, near which combustion is intense and stable. Right after staging, despite having a mean equivalence ratio of 0.45, the pilot flame maximum local equivalence ratio reaches roughly 0.75 which also provides certain stability [31].

3.3 Alternative Calibrations

Besides the calibrated model above, it is interesting to explore other alternative models that can potentially reproduce the EEDB NO_x and CO emissions. Specifically of interest are those models with pilot fuel fractions between 0% and 30%, because multiple previous studies found the minimum NO_x pilot fuel fraction existed within that range [18, 19, 20]. Hence, shown in Figure 3-7 and 3-8 are five alternative models with different pilot fuel fractions.

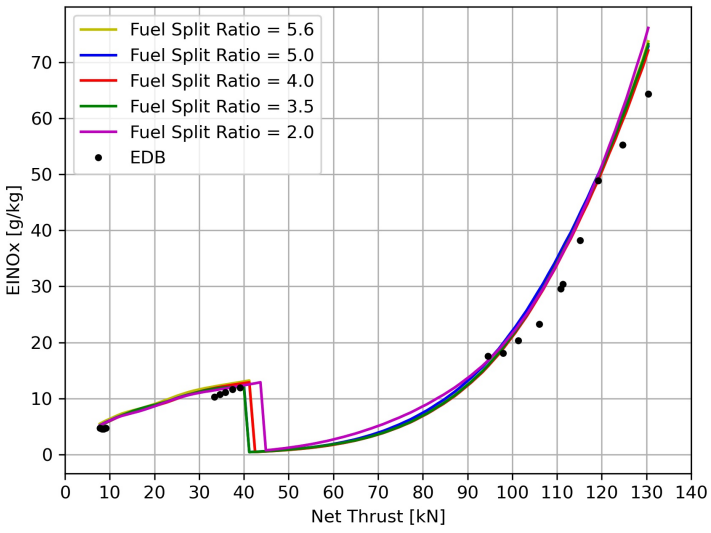

Figure 3-7: Alternative lean-burn staged combustor models - NO_x emissions

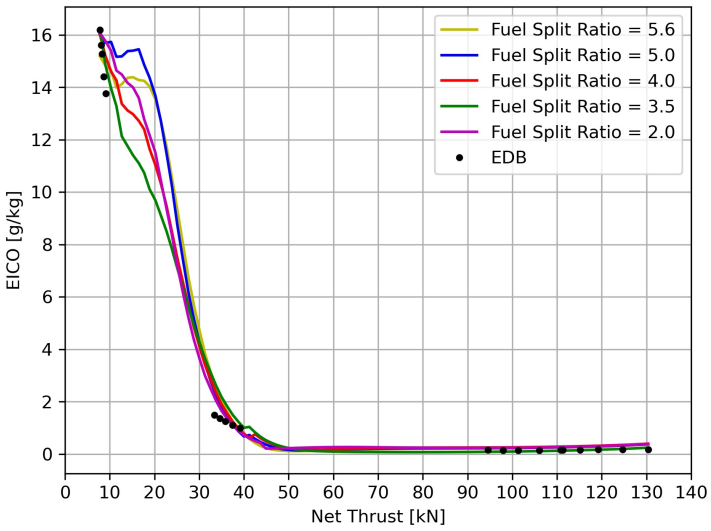

Figure 3-8: Alternative lean-burn staged combustor models - CO emissions

Lines are plotted in these figures purely for readability purpose since continuous results are never produced out of these models. The fuel split ratio again is defined as the main flame fuel flow rate over the pilot, and the fuel split ratios of 5.6, 5.0, 4.0, 3.5, and 2.0 correspond to pilot fuel fractions of 15%, 16%, 20%, 22%, and 33% respectively. Even though the predicted NO_x emissions of these alternative models match with the EEDB results well, their CO emissions during low power operation deviate from the experimental results. Hence, they are not selected for further analysis.

The differences between these models can also be seen from their dome equivalence ratios evolution in Figure 3-9 and 3-10. The main flame equivalence ratios between these models are similar to each other and are constructed such that they maintain low power stability and high power low NO_x emissions. However, it can be seen that as the pilot flame fuel fraction decreases toward 15%, the pilot flame equivalence ratio right after staging becomes leaner. At the pilot fuel fraction of 15%, the minimum mean equivalence ratio reaches 0.2, which can cause blow-out in real life.

The reason behind this phenomenon is that as the pilot fuel fraction decreases, the pilot air fraction also decreases, if a stable combustion after staging needs to be

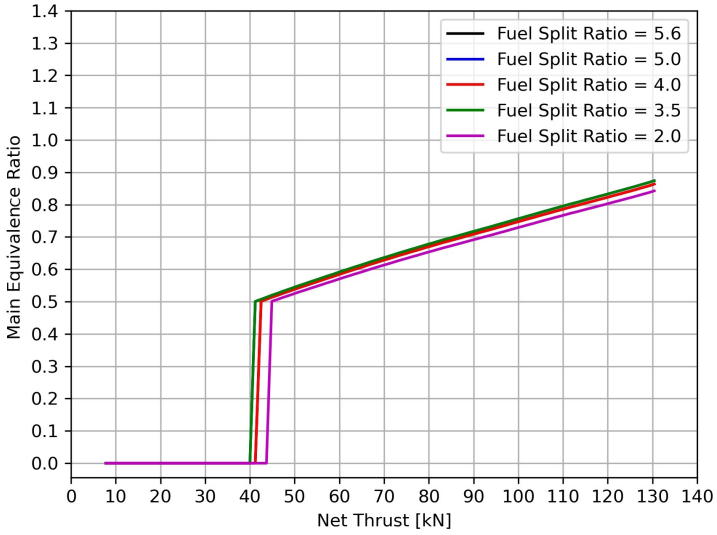

Figure 3-9: Main equivalence ratio for alternative lean-burn staged combustor models

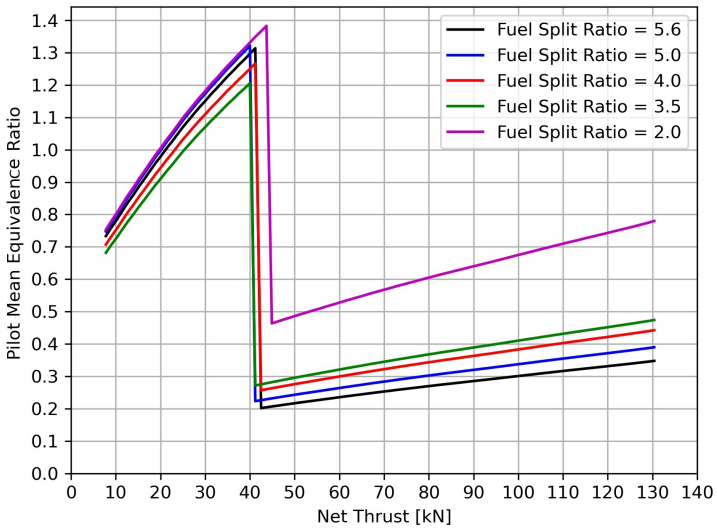

Figure 3-10: Pilot equivalence ratio for alternative lean-burn staged combustor models

maintained. However, as only the pilot fuel injector is used before staging, decreasing the pilot air fraction would make the pilot flame very rich in pilot-only mode, susceptible to high CO and soot emissions. This prevents the model-predicted EI_{CO} from matching with the EEDB data. Therefore, for those high fuel split ratio cases, in order to match with the low power CO emissions experimentally measured, the pilot

air fraction has to be maintained comparatively high, and the pilot mean equivalence ratio comparatively lean during the high power operation. This phenomenon makes the use of a pilot fuel fraction less than 30% unfavorable for the current study.

3.4 Impact of Staging on Emissions

As the EEDB only provides NO_x emissions for the LTO thrust levels, NO_x emissions during other throttle conditions are not known. Therefore, the lean-burn staged combustor model in the section is run at the sea-level static conditions across all power levels from 0% to 100% rated thrust to predict the full profile of NO_x emissions. Moreover, the NO_x emissions before and after staging are compared.

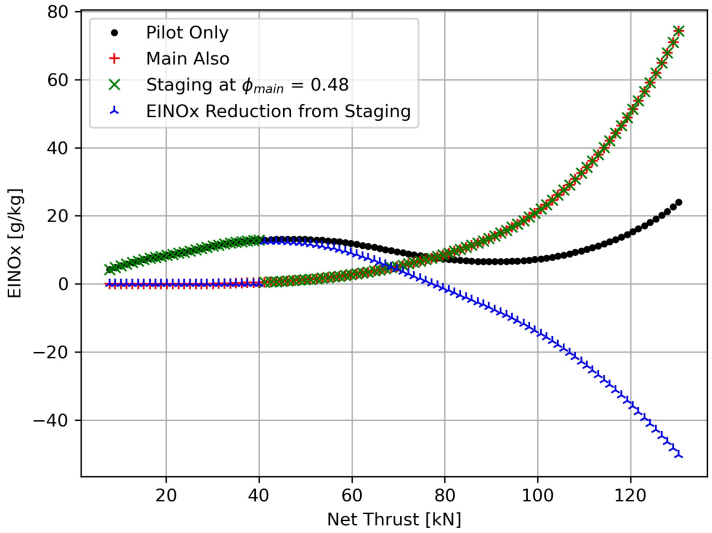

Figure 3-11: Effects of staging on NO_x emissions - ground operation

Figure 3-11 shows the NO_x emissions predicted by the lean-burn staged combustor model at the sea-level static conditions. The main-also operation represents the scenario that both the main and the pilot fuel injectors are switched on across all the throttle conditions, and vice versa for the pilot-only operation. Staging at the main equivalence ratio of 0.48 is the calibrated case. The EI_{NO_x} reduction from staging is the difference in EI_{NO_x} between the calibrated case and the pilot-only case. 30% rated

thrust is where the maximum NO_x reduction from staging can be obtained. It has a benefit of reducing EI_{NO_x} to 0.5 g/kg. However, as the thrust level increases, the staging NO_x reduction benefit decays, and no benefit exists at around 80 kN thrust level or 60% rated thrust. The predicted NO_x emissions for the high-power pilot-only operation and the low-power main-also operation are highly uncertain due to the lack of experimental data about the combustor operating in those conditions. Overall, Figure 3-11 suggests that staging should occur as early as allowed by stability to maximize the NO_x reduction benefit, and the benefit decays as thrust increases.

To observe how staging reduces the NO_x emissions, the local temperature, pressure, and equivalence ratio within the combustor are plotted in Figure 3-12.

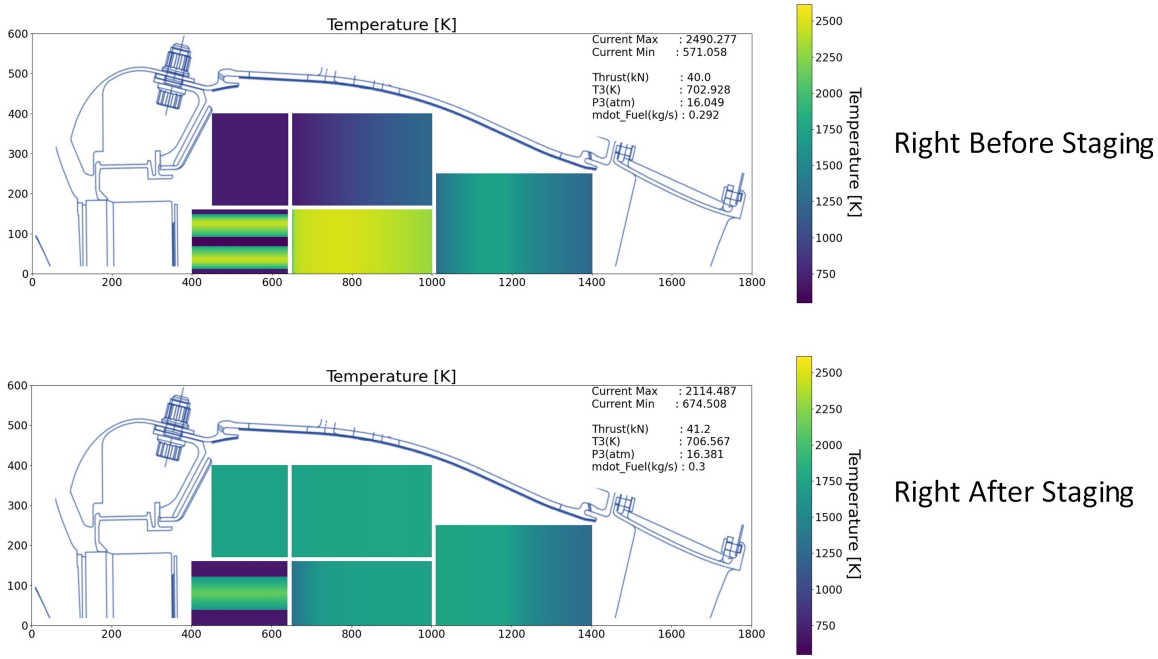

Figure 3-12: Effect of staging on temperature field

Each block in Figure 3-12 represents a reactor, and the locations of blocks correspond to the reactor network layout in Figure 2-2. The color represents the temperature based on the color bar to the right, while the thrust levels are 40 kN and 41.2 kN which are before and after staging. Dimensions are not scaled and do not indicate relative volumes. For the two WSRs at the dome, color is distributed across different sub-WSRs, while for the rest of the PFRs to the end, color is distributed

across different axial locations. Right before staging, all the fuel is injected into the pilot flame, and the two bright yellow bars in the pilot root WSR represent the stoichiometric regions in the diffusion flame. The local temperature reaches a maximum of 2500 K in the pilot tail PFR, as the combined mixing flow from the main tail PFR triggers the oxidation of CO. This is consistent with the RQL combustion process indicated by Brink [23]. Right after staging, as the main fuel injector is turned on, both the pilot and the main flame are burning lean, while a near stoichiometric region can still be seen from the pilot root WSR to maintain combustion stability. A more important feature to be observed is how the maximum local temperature drops from 2496 K to 2114 K through the staging process. Instead of having a concentrated high temperature zone before staging, the temperature field becomes uniform after staging.

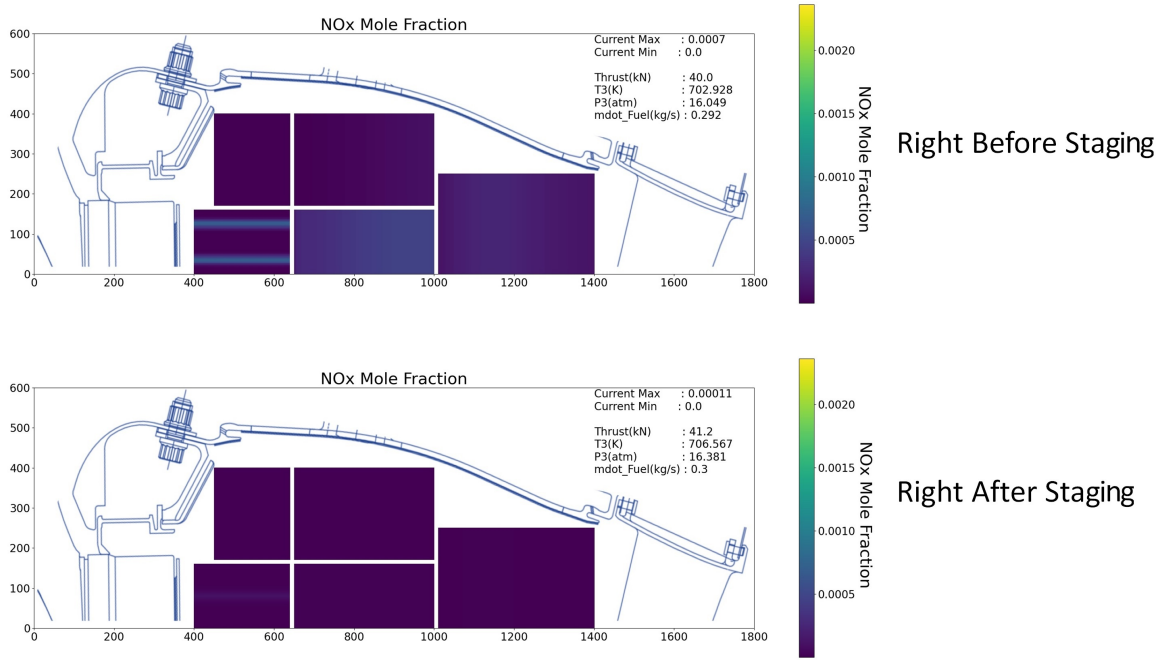

Figure 3-13: Effect of staging on NO_x concentration

The effects of a uniform and low temperature field after staging on the NO_x emissions can be seen from Figure 3-13. The same layout of reactors is shown, while the color in Figure 3-13 represents the mole fraction of NO_x. In this case, NO_x includes NO_2 and NO. It can be observed that the high NO_x concentration regions correspond

to the high temperature regions from Figure 3-12. Hence, as the maximum temperature drops after staging, the high NO_x concentration regions also disappear with the maximum local NO_x mole fraction dropping from 0.0007 to 0.0001. Therefore, staging reduces NO_x emissions by diffusing the concentrated high temperature field into a more uniform low temperature field.

3.5 Flight Mission Emissions Analysis

The above section considers the sea-level static operation of the lean-burn staged combustor. To simulate the in-flight combustor performance, TASOPT flight mission parameters are used to generate the combustor inlet conditions. The EI_{NO_x} during different phases of flight can be seen in Figure 3-14. The combustor operates on main-also mode for takeoff, climb-out, and cruise, while on pilot-only mode for descent.

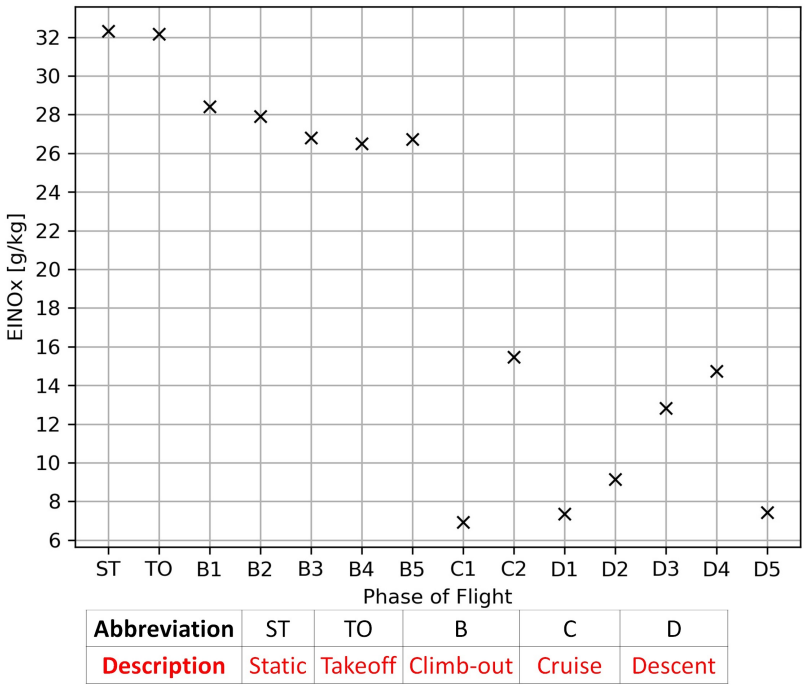

Figure 3-14: Lean-burn staged combustor in-flight NO_x emissions

The EI_{NO_x} are between 26 g/kg and 33 g/kg during takeoff and climb-out, and between 6 g/kg and 16 g/kg during cruise and decent. The first cruise operation (C1)

has an EI_{NO_x} of 7 g/kg which is consistent with the CLEEN program report [12] that cruise EI_{NO_x} is less than 9 g/kg.

3.6 Optimizing the Fuel Split Ratio

The section above only considers a fixed fuel split ratio after staging. This section studies how varying fuel split ratio would affect the NO_x emissions.

The fuel split ratio is defined as the ratio of the main zone fuel flow rate over the pilot zone fuel flow rate. At sea-level static conditions across all throttle levels with a fixed air distribution and a constant combustor geometry, the fuel split ratio is varied from 0 to 5, corresponding to the a pilot fuel fraction from 100% to 16%. The EI_{NO_x} of each case is then calculated, and the fuel split ratio corresponding to the minimum EI_{NO_x} at each throttle condition is labeled as shown in Figure 3-15.

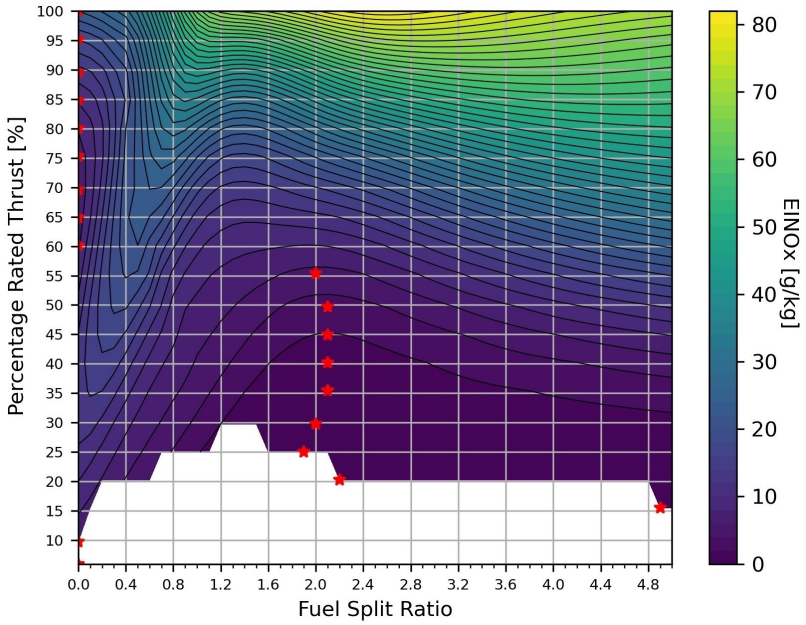

Figure 3-15: Optimizing the Fuel Split Ratio

For the vertical axis, the rated thrust is 130 kN. The white space on the bottom represents the region where blow-out occurs. Pilot-only operation is assumed for power levels below 30% rated thrust to maintain combustion stability. The red dots indicate the optimal fuel split ratio at each thrust level where the minimum EI_{NO_x}

can be achieved.

For power levels above 30% rated thrust, it is observed that though fuel split ratios can vary freely, the optimal ratios are roughly constant.

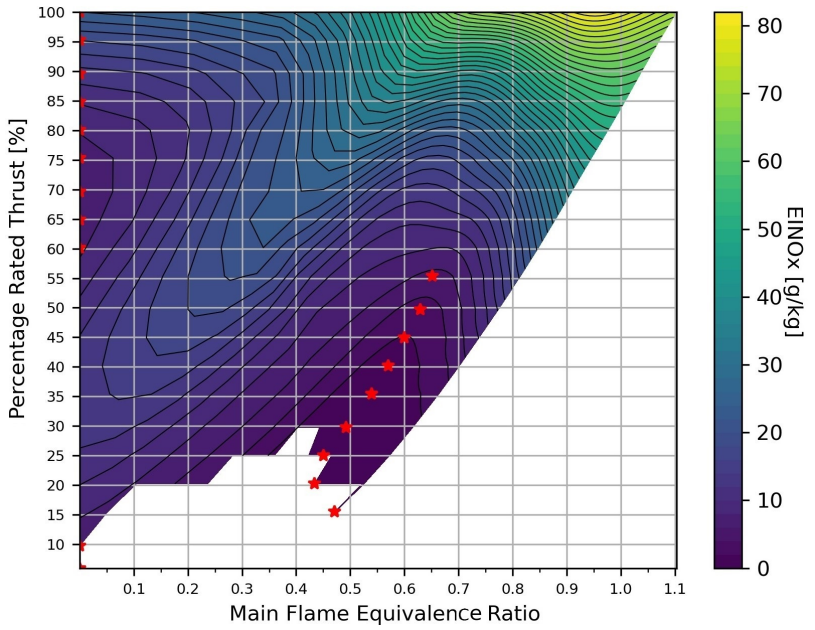

Figure 3-16: Evolution of the optimal main flame equivalence ratio

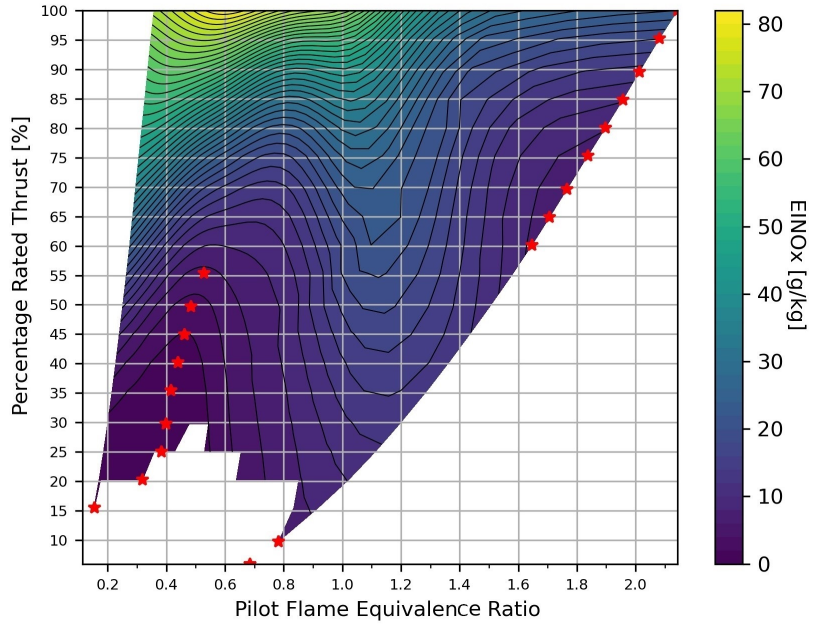

Figure 3-17: Evolution of the optimal pilot flame equivalence ratio

Figures 3-16 and 3-17 show the evolution of the pilot and main equivalence ratios.

Red dots correspond to the optimal fuel split ratios. It is consistent with the previous study by Li et al. [20] that if the main flame equivalence ratio is above 0.69, further decreasing the pilot fuel split ratio can cause NO_x emissions to increase. However, as opposed to varying the fuel split ratio such that the main equivalence ratio is kept constant at 0.69 as suggested by Li et al., it is found that the optimal main equivalence ratio for minimum NO_x emissions actually varies between 0.5 and 0.65. The corresponding pilot mean equivalence ratio varies from 0.4 to 0.55. The white space is the infeasible region where blow-out occurs.

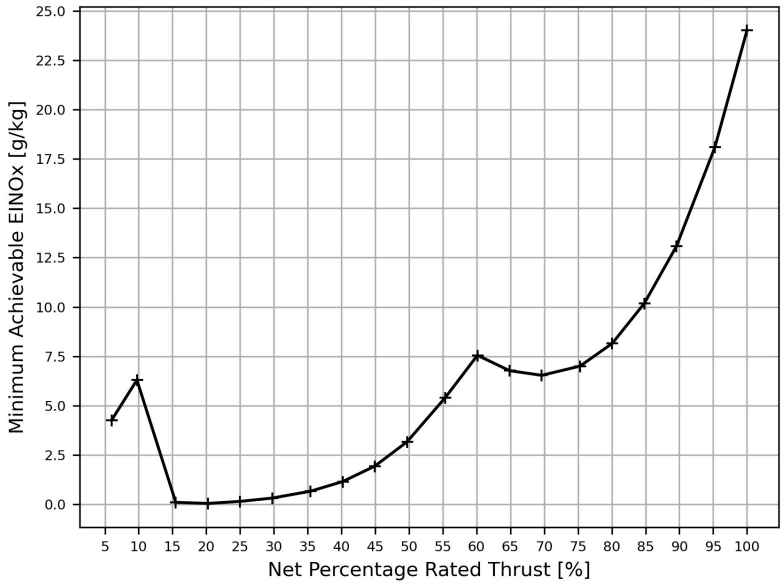

Figure 3-18: Minimum achievable EI_{NO_x} from varying the fuel split ratio

Figure 3-18 shows the minimum achievable EI_{NO_x} from varying the fuel split ratio. Data from Figure 3-18 below the 30% rated thrust might be infeasible, because the combustor model does not predict combustion stability. Two EI_{NO_x} trends during high power operation are observed. This forms the basis for the hypothesis for the two EI_{NO_x} trends in the LEAP-1B engine EEDB data shown previously in Figures 2-6, 3-4, and 3-7, against which a fixed fuel split ratio model cannot match perfectly. The hypothesis is that the LEAP-1B engine might be using multiple fuel split ratios to minimize NO_x emissions.

Also of interest is how the air split ratio affects the optimal fuel split ratio. Analysis

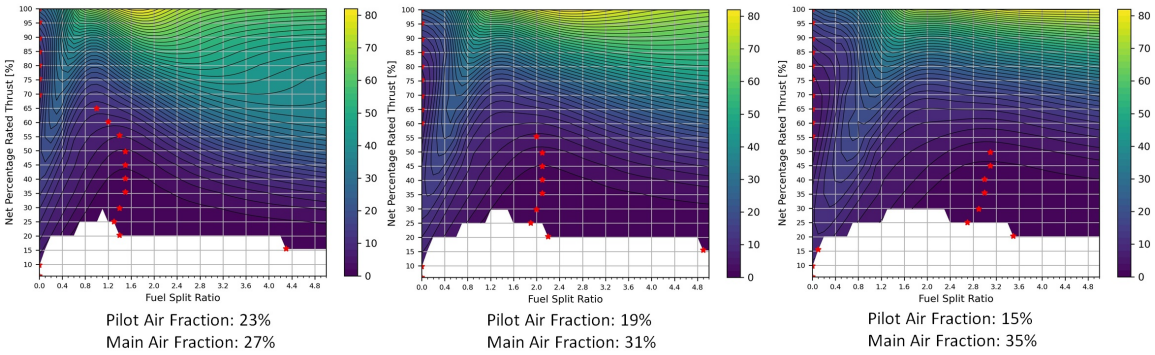

Figure 3-19: Effects of combustor dome air distribution on the optimal fuel split ratios

is performed by keeping the 50% cooling air unchanged from the calibrated model, but only varying the air split between the pilot and the main flame. The results are shown in Figure 3-19. The plot in the center is the calibrated model, while from left to right the air distributed to the pilot flame decreases in steps of 4%. As pilot air decreases, the contour plot is stretched to the right, increasing the optimal fuel split ratios.

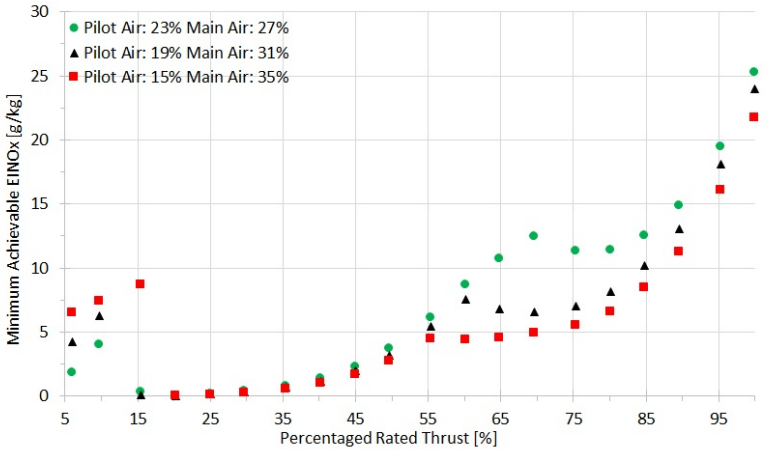

Figure 3-20: Effects of dome air distribution on the minimum achievable EI_{NO_x}

Figure 3-20 shows the effects of the combustor dome air distribution on the minimum achievable EI_{NO_x}. Data from Figure 3-20 below the 30% rated thrust might be infeasible, because the combustor model does not predict combustion stability. It is observed that reducing the air flow to the pilot flame reduces the overall EI_{NO_x} level.

3.7 RQL Emissions Comparison

Because the pilot-only mode of the lean-burn staged combustor resembles an RQL combustion process, an interesting question to ask is whether lean-burn staged combustor can outperform RQL combustor in terms of NO_x emissions. This section performs a comparison of the NO_x emission performance of an RQL combustor against the lean-burn staged combustor, with both combustor models running on the same engine cycle.

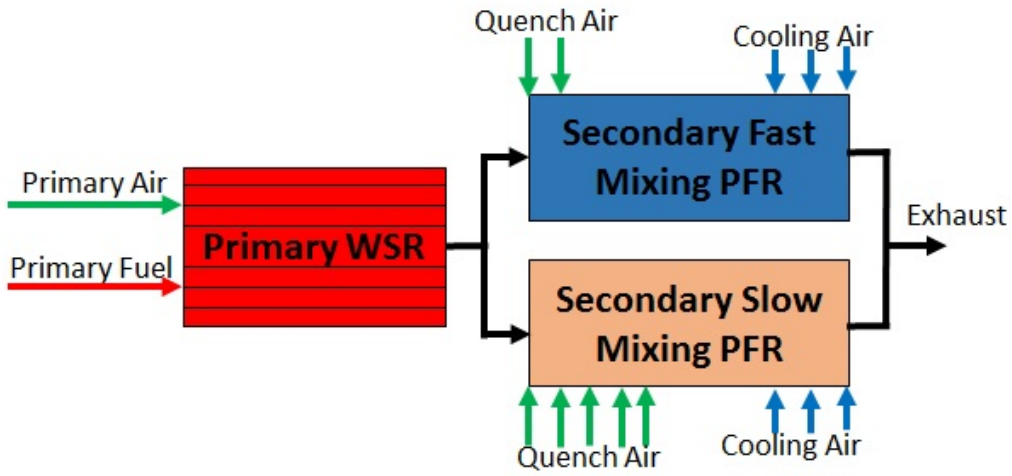

Figure 3-21: RQL combustor chemical reactor network

An RQL combustor chemical reactor network from Brink [23] is used with its schematic shown in Figure 3-21. The model is validated against the EEDB CFM56-5B engine NO_x and CO emissions. The calibrated results are shown in Figures 3-22 and 3-23. The relative RMS errors are 0.61% and 0.74%, respectively.

This analysis uses the TASOPT flight mission and NPSS engine cycle model corresponding to the previous calibrated lean-burn staged combustor model. The same representative flight mission and calibrated NPSS engine cycle model are used for both the calibrated lean-burn staged combustor model and the RQL combustor model. Then, the resulting EI_{NOx} from the two combustor models are compared. The differences in EI_{NOx} come purely from the combustor design.

For sea-level static conditions, a comparison between the EI_{NO_x} performance of

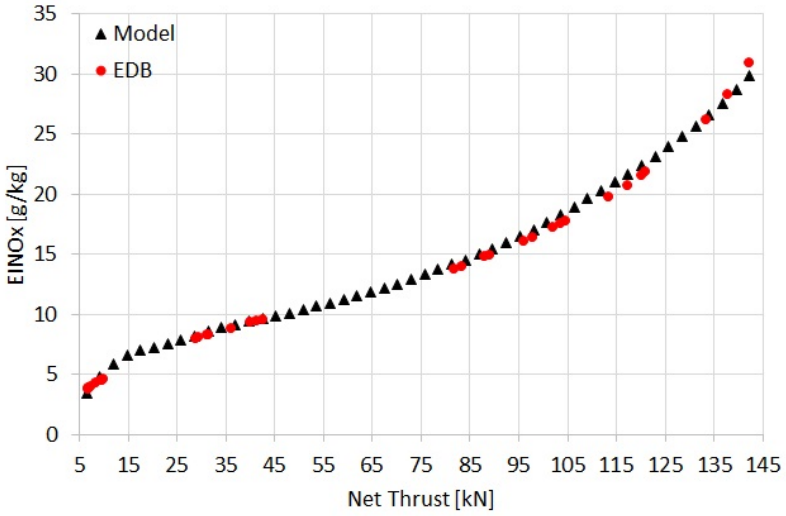

Figure 3-22: RQL combustor NO_x emissions calibration

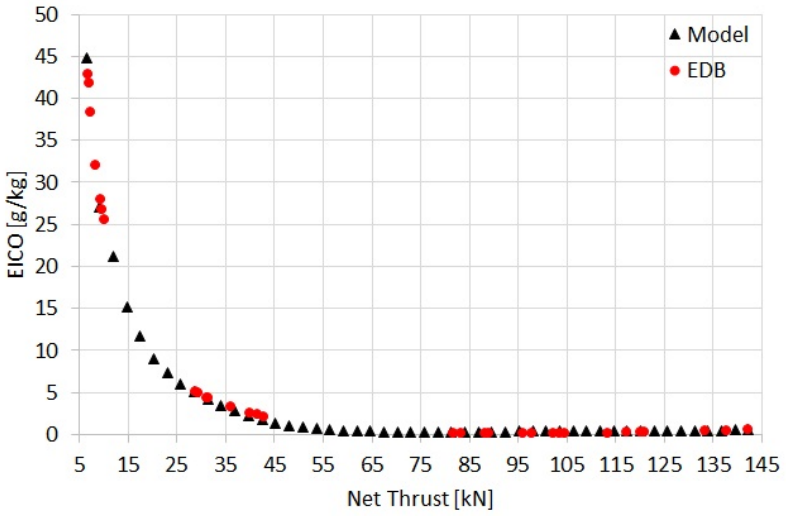

Figure 3-23: RQL combustor CO emissions calibration

both combustors is shown in Figure 3-24. "Difference" is the difference in EI_{NO_x} between the two combustors. It is observed that through most of the operating conditions, the lean-burn staged combustor performs better than the RQL combustor. Right after staging, roughly a 20 g/kg EI_{NO_x} reduction benefit is obtained by using staged combustor. As the thrust increases, a maximum 30 g/kg EI_{NO_x} reduction benefit from staged combustor is achieved at around 90 kN thrust point. As thrust keeps increasing towards 100%, a crossover point shows up at around 127 kN.

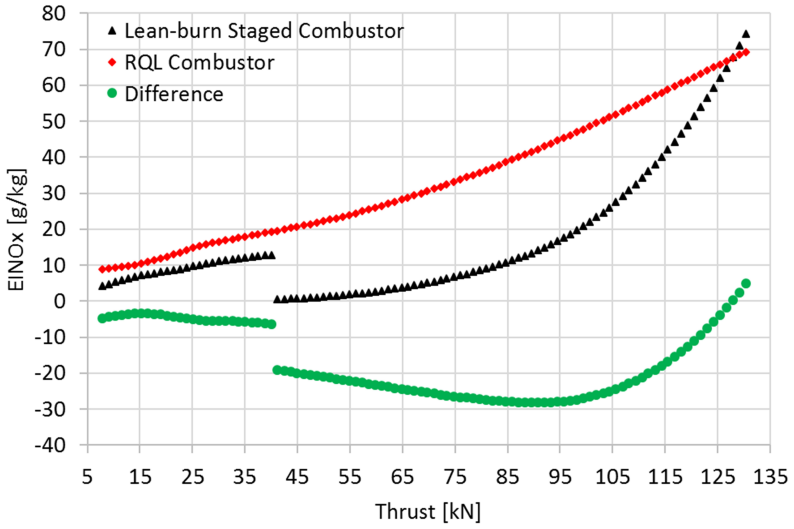

Figure 3-24: SLS EI_{NO_x} of RQL and lean-burn staged combustors

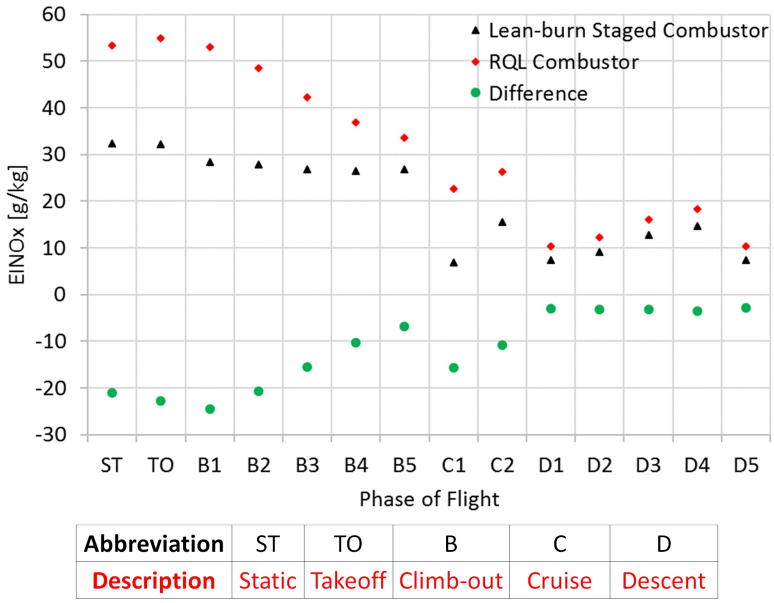

Abbreviation	ST	TO	B	C	D
Description	Static	Takeoff	Climb-out	Cruise	Descent

Figure 3-25: In-flight EI_{NO_x} of RQL and lean-burn staged combustors

Using the flight mission, a comparison of the in-flight EI_{NO_x} performance of the two combustors is shown in Figure 3-25. An EI_{NO_x} reduction benefit from using staged combustor is observed through all phases of flight. Overall, at both the sea-level static and in-flight conditions, significant benefits from staging are observed when using a lean-burn staged combustor over an RQL combustor, making the lean-burn staged

combustor a promising NO_x reduction solution.

Chapter 4

Conclusions

Using chemical reactor networks, NPSS engine cycle models, and a TASOPT flight mission model, this thesis investigates the effects of a lean-burn staged combstor staging and fuel split ratio on NO_x emissions through a sea-level static and a flight mission analysis. NO_x reduction benefits from optimizing the fuel split ratio are studied, and the EI_{NO_x} performance between an RQL and a lean-burn staged combustor are compared. In comparison to previous studies, a wider range of pilot fuel fraction, from 16% to 100%, are tested over more refined thrust cases, from 0% to 100% rated thrust. A wider range of phases, including the cruise conditions in addition to the LTO cycle, are employed in this thesis.

Through the exploration of different alternative calibrated combustor models, it is found that a pilot fuel fraction between 10% and 20% is not feasible, because the pilot flame after staging is too lean to be maintained. From analysis at the sea-level static conditions, staging should occur as early as allowed by stability to reduce NO_x emissions, and the NO_x reduction benefit decays as thrust increases. The NO_x reduction benefit from staging is also found to result from the creation of a low and uniform temperature field.

When optimizing the fuel split ratio to minimize NO_x emissions, it is found that the optimal ratios are roughly constant with varying thrust. Moreover, it is found consistent with a previous study [20] that the optimal main flame equivalence ratio is never higher than 0.69 for minimum NO_x emissions. However, instead of being a con-

stant at 0.69 as indicated by the previous study, the optimal main flame equivalence ratio varies between 0.5 and 0.65. In addition, a hypothesis for the use of variable fuel split ratio by LEAP-1B engine is proposed.

When letting the combustor dome air distribution vary, it is found that a decrease of air distributed to the pilot flame results in a higher optimal fuel split ratio or a lower pilot fuel fraction. In addition, as the pilot air flow decreases, a decrease in the overall EI_{NO_x} level is observed.

Lastly, through a comparison between the EI_{NO_x} performance between an RQL and a lean-burn staged combustors, it is found that at both the sea-level static and in-flight conditions, significant staging NO_x reduction benefit is resulted by using a lean-burn staged combustor over an RQL combustor, making the lean-burn staged combustor a promising NO_x reduction solution.

For future study, the hypothesis and conclusions proposed in this thesis need to be further investigated and validated by obtaining a calibrated combustor model with a variable fuel split ratio. Especially given the existence of many alternative models, further constraints in terms of experimental data, such as the variation of the combustor air distribution with respect to the fuel flow rate, might be needed to more firmly validate the staged combustor model. Moreover, the combustor model can be used in the future to predict HC and nvPM emissions and to study the effects of different fuel types on the emission performance of the staged combustor.

Bibliography

[1] Hoermann, W. ICAO aircraft engine emissions databank. https://www.easa.europa.eu/domains/environment/icao-aircraft-engine-emissions-databank/, 2021.

[2] Yu, W., Tay, K., Zhao, F., Yang, W., Li, H. and Xu, H. Development of a new jet fuel surrogate and its associated reaction mechanism coupled with a multistep soot model for diesel engine combustion. *Applied Energy*, 2018.

[3] Turns, S.R. *Introduction to combustion.* New York, NY, USA: McGraw-Hill Companies, 1996.

[4] Yim, S.H., Lee, G.L., Lee, I.H., Allroggen, F., Ashok, A., Caiazzo, F., Eastham, S.D., Malina, R. and Barrett, S.R. Global, regional and local health impacts of civil aviation emissions. *Environmental research letters*, 2015.

[5] Barrett, S.R., Britter, R.E. and Waitz, I.A. Global mortality attributable to aircraft cruise emissions. *Environmental science and technology*, 2010.

[6] Brasseur, G.P., Cox, R.A., Hauglustaine, D., Isaksen, I., Lelieveld, J., Lister, D.H., Sausen, R., Schumann, U., Wahner, A. and Wiesen, P. European scientific assessment of the atmospheric effects of aircraft emissions. *Atmospheric Environment*, 1998.

[7] Eastham, S.D. and Barrett, S.R. Aviation-attributable ozone as a driver for changes in mortality related to air quality and skin cancer. *Atmospheric Environment*, 2016.

[8] Mounir, I. Commercial market outlook 2021–2040. https://www.boeing.com/commercial/market/commercial-market-outlook/, 2021.

[9] Schaffrath, S. Airbus foresees demand for 39,000 new passenger freighter aircraft by 2040. https://www.airbus.com/en/newsroom/press-releases/2021-11-airbus-foresees-demand-for-39000-new-passenger-freighter-aircraft/, 2021.

[10] William, R.C. 2021 global air passenger totals show improvement from 2020, but still only half pre-pandemic levels. https://www.icao.int/Newsroom/Pages/2021-global-air-passenger-totals-show-improvement.aspx/, 2022.

[11] Liu, Y., Sun, X., Sethi, V., Nalianda, D., Li, Y.G. and Wang, L. Review of modern low emissions combustion technologies for aero gas turbine engines. *Progress in Aerospace Sciences*, 2017.

[12] Stickles, R., Barrett, J. and Jefferies, R. TAPS II combustor final report. Technical report, General Electric, 2013.

[13] Yamamoto, T., Shimodaira, K., Kurosawa, Y., Yoshida, S. and Matsuura, K. Investigations of a staged fuel nozzle for aeroengines by multi-sector combustor test. In *Turbo Expo: Power for Land, Sea, and Air*, 2010.

[14] Yamamoto, T., Shimodaira, K., Kurosawa, Y. and Yoshida, S. Combustion characteristics of fuel staged combustor for aeroengines at LTO cycle conditions. In *Turbo Expo: Power for Land, Sea, and Air*, 2011.

[15] Yamamoto, T., Shimodaira, K., Yoshida, S. and Kurosawa, Y. Emission reduction of fuel-staged aircraft engine combustor using an additional premixed fuel nozzle. *Journal of engineering for gas turbines and power*, 2013.

[16] Fu, Z., Lin, Y., Li, L. and Zhang, C. Experimental and numerical studies of a lean-burn internally-staged combustor. *Chinese Journal of Aeronautics*, 2014.

[17] Zhichao, W., Yuzhen, L., Jianchen, W., Zhang, C. and Zhijun, P. Experimental study on NOx emission correlation of fuel staged combustion in a LPP combustor at high pressure based on NO-chemiluminescence. *Chinese Journal of Aeronautics*, 2020.

[18] Cheng, M., Shang, S.T., Liu, D.C., Gao, J.C., Guo, R.Q., Zhang, S.S. and Li, F. Influence of fuel-staging ratio on TAPS combustor performance. *Aeroengine*, 2012.

[19] Liu, F., Zhang, K., Liu, C., Mu, Y., Yang, J., Xu, G. and Zhu, J. Numerical and experimental investigation on emission performance of a fuel staged combustor. *Science China Technological Sciences*, 2014.

[20] Li, L., Lin, Y., Fu, Z. and Zhang, C. Emission characteristics of a model combustor for aero gas turbine application. *Experimental Thermal and Fluid Science*, 2016.

[21] Han, D.S., Kim, G.B., Kim, H.S. and Jeon, C.H. Experimental study of NOx correlation for fuel staged combustion using lab-scale gas turbine combustor at high pressure. *Experimental thermal and fluid science*, 2014.

[22] Zhao, T., Liu, X., Zheng, H., Zhang, Z., Yang, J. and Li, Z. Effect of fuel stage proportion on flame position in an internally-staged combustor. In *Turbo Expo: Power for Land, Sea, and Air*, 2020.

[23] Brink, L.F.J. Modeling the impact of fuel composition on aircraft engine NOx, CO and soot emissions. Master's thesis, Massachusetts Institute of Technology, 2020.

[24] Martini, B. *Development and assessment of a soot emissions model for aircraft gas turbine engines.* PhD thesis, Massachusetts Institute of Technology, 2008.

[25] Allaire, D.L. *A physics-based emissions model for aircraft gas turbine combustors.* PhD thesis, Massachusetts Institute of Technology, 2006.

[26] Moniruzzaman, C.G. and Yu, F. A 0D aircraft engine emission model with detailed chemistry and soot microphysics. *Combustion and Flame*, 2012.

[27] Bisson, J., Seers, P., Huegel, M. and Garnier, F. Numerical prediction of gaseous aerosol precursors and particles in an aircraft engine. *Journal of Propulsion and Power*, 2016.

[28] Temme, J.E., Allison, P.M. and Driscoll, J.F. Combustion instability of a lean premixed prevaporized gas turbine combustor studied using phase-averaged PIV. *Combustion and Flame*, 2014.

[29] Dhanuka, S.K., Temme, J.E. and Driscoll, J.F. Unsteady aspects of lean premixed prevaporized gas turbine combustors: flame-flame interactions. *Journal of Propulsion and Power*, 2011.

[30] Zhang, Q., Xu, H.S., Gui, T., Sun, S.L., Wu, Y. and Yan, D.B. Investigation on reaction flow field of low emission TAPS combustors. *Applied Mechanics and Materials*, 2014.

[31] Huang, Y. and Yang, V. Bifurcation of flame structure in a lean-premixed swirl-stabilized combustor: transition from stable to unstable flame. *Combustion and Flame*, 2004.

[32] Heywood, J.B. and Mikus, T. Parameters controlling nitric oxide emissions from gas turbine combustors. In *AGARD Propulsion and Energetics Panel 41st Meeting on Atmospheric Pollution by Aircraft Engines*, 1973.

[33] Fletcher, R. and Heywood, J. A model for nitric oxide emission from aircraft gas turbine engines. In *9th Aerospace Sciences Meeting*, 1971.

[34] Goodwin, D.G., Moffat, H.K., Schoegl, I., Speth, R.L. and Weber, B.W. Cantera: An object-oriented software toolkit for chemical kinetics, thermodynamics, and transport processes. https://www.cantera.org, 2022. Version 2.6.0.

[35] Cumpsty, N. and Heyes, A. *Jet propulsion.* Cambridge University Press, 2015.

[36] Kerrebrock, J.L. *Aircraft engines and gas turbines.* MIT Press, 1992.

[37] Brown, P.N., Byrne, G.D. and Hindmarsh, A.C. VODE: A variable-coefficient ODE solver. *SIAM journal on scientific and statistical computing*, 1989.

[38] Pejpichestakul, W., Cuoci, A., Frassoldati, A., Pelucchi, M., Parente, A. and Faravelli, T. Buoyancy effect in sooting laminar premixed ethylene flame. *Combustion and Flame*, 2019.

[39] Pejpichestakul, W., Ranzi, E., Pelucchi, M., Frassoldati, A., Cuoci, A., Parente, A. and Faravelli, T. Examination of a soot model in premixed laminar flames at fuel-rich conditions. In *Proceedings of the Combustion Institute*, 2019.

[40] Bagheri, G., Ranzi, E., Pelucchi, M., Parente, A., Frassoldati, A. and Faravelli, T. Comprehensive kinetic study of combustion technologies for low environmental impact: MILD and OXY-fuel combustion of methane. *Combustion and Flame*, 2020.

[41] Ranzi, E., Frassoldati, A., Stagni, A., Pelucchi, M., Cuoci, A. and Faravelli, T. Reduced kinetic schemes of complex reaction systems: fossil and biomass-derived transportation fuels. *International Journal of Chemical Kinetics*, 2014.

[42] Ranzi, E., Cavallotti, C., Cuoci, A., Frassoldati, A., Pelucchi, M. and Faravelli, T. New reaction classes in the kinetic modeling of low temperature oxidation of n-alkanes. *Combustion and Flame*, 2015.

[43] Hoermann, W. Introduction to the ICAO engine emissions databank. https://www.easa.europa.eu/domains/environment/icao-aircraft-engine-emissions-databank/, 2021.

[44] Jones, D.R., Perttunen, C.D. and Stuckman, B.E. Lipschitzian optimization without the Lipschitz constant. *Journal of optimization Theory and Applications*, 1993.

[45] Gablonsky, J.M.X. *Modifications of the DIRECT algorithm.* North Carolina state university, 2001.

[46] Drela, M. TASOPT 2.00. tech. rep. Technical report, Massachusetts Institute of Technology, 2010.

[47] Jones, S.M. An introduction to thermodynamic performance analysis of aircraft gas turbine engine cycles using the numerical propulsion system simulation code, 2007.

[48] Prashanth, P. Personal communication, 2022.

[49] Greitzer, E.M., Bonnefoy, P.A., DelaRosaBlanco, E., Dorbian, C.S., Drela, M., Hall, D.K., Hansman, R.J., Hileman, J.I., Liebeck, R.H., Lovegren, J. and Mody, P. N+ 3 aircraft concept designs and trade studies, 2010.

[50] Brady, C. The 737 information site. http://www.b737.org.uk/, 1999.